Induced changes in protein secondary structure due to internal sequence modifications and ligand binding

A THESIS SUBMITTED TO THE FACULTY OF THE
UNIVERSITY OF MINNESOTA BY

Katie Dunleavy

IN PARTIAL FULFILLMENT OF THE REQUIREMENTS FOR THE DEGREE OF
MASTER OF SCIENCE

Dr. Anne Hinderliter

September 2015

Acknowledgements:

I would like to thank Dr. Anne Hinderliter for allowing me the opportunity to explore the field of biochemistry over the past two years in the graduate program. If not given the chance to explore research within her laboratory, I would not have found my passion for the field of chemistry and biochemistry. I am grateful for her patience and constant encouragement throughout my time at the University of Minnesota Duluth. This work could not have been completed if not for the constant support from my fellow graduate students, Ryan Mahling, Benjamin Horn, Stephanie Kobany and Benjamin Orpen. I am also grateful for the work and support from all the undergraduate students who have worked in the Hinderliter lab during my time here. A special thanks is owed to Michael Fealey, as his support and advice from afar was helpful in the progression of this project. I have received great instructional guidance from Dr. John Evans, of whom I am thankful for the patience and advice that he has contributed both to this project and to the growth of my education. Lastly, I would like to thank Dr. Jonathan Sachs, for allowing me to collaborate on the α-synuclein project that has been recently introduced to the Hinderliter lab. I am honored to have contributed to the growth of this collaboration.

Abstract:

Secondary structure of protein sequences is dependent on both internal and external interactions of amino acid residues and ligand-binding partners. Internal residue features can leave a protein in an ordered, folded state, or in a disordered, unfolded state. Structural characteristics can be further influenced by protein-ligand binding interactions with a lipid membrane surface. Structural features can be altered upon membrane binding, causing disordered proteins to become more ordered in structure. The stabilizing influence of methionine (Met) oxidation in an aromatic-Met hydrogen bonding interaction, within a small, 15-residue peptide was studied using Differential Scanning Calorimetry (DSC) and Circular Dichroism (CD) Spectroscopy to observe changes in structural strength. By observing the ordered to disordered transition of this peptide, changes in enthalpy and transition temperature were determined. This added aromatic-oxidized Met interaction causes a stronger and more stable ordered peptide structure due to internal residue interaction. Multiple intrinsically disordered proteins were studied upon binding to a membrane surface to determine the influence that physiological membrane surfaces and curvature have on appropriate conformer formation of synaptic vesicle (SV) binding proteins. Various C2 domains of synaptotagmin I (Syt I) and α-Synuclein (αS) were studied using DSC, CD and Carboxyfluorescein (CF) release assays. The proper folding of these proteins is important for their necessary function, and misfolding or sequence mutation can significantly alter their functionality within neuronal environments. These studies are vital to enhance understanding of the dependence of internal residue and membrane binding interactions on structural properties of proteins, as these specific interactions are not limited to individual systems.

Table of Contents:

List of Tables:

Table 4.4: Calculated enthalpy (ΔH), heat capacity change (ΔCp), melting temperature (Tm) and free energy at body temperature ($\Delta G_{37°C}$) values for 20μM αS in the presence of SV mimicked SUVs at a 200:1 [L]:[P] ratio, from Figure 4.6 heating thermogram.

List of Figures:

mM EGTA (**dashed blue line**). The large ΔCp differences are highlighted for the C2A domain with brackets (left panel). The right panel is the CD spectrum obtained for the C2A domain (residues 96-265) in the presence of 700 μM LUVs composed of POPC:POPS (60:40) and 1mM Ca2+. ***Lower Panels:*** The left panel shows the free energies stabilities of several C2 domains, in the absence of ligand, over a range of temperatures. These stabilities were calculated through the use of the Gibbs-Helmholtz equation, utilizing the ΔH, ΔCp, and Tm obtained from the thermal denaturation profiles of the domains. The **orange triangles**, **red squares**, **blue squares**, **green circles** and **black circles** represent canonical C2A Dys, C2Av1 Dys, human Syt I C2A (residues140-265), cotton Syt I C2A, and human Syt I C2B, respectively. The right panel shows the denaturation profile of the cotton C2A domain [Cotton C2A] = 175μM) with that of the human Syt I C2A domain construct containing the amino acids 140-265 (blue; [Human C2A] = 13μM) in the presence of 1mM EGTA. The **blue** and **green** lines under the curves represent the baselines used for integration.

Figure 3.4: ***Left Panel*****:** Thermograms obtained for LUVs of the membrane domain forming lipid mixture, at a phospholipid concentration of 3.3mM (**solid black line**) and the SV mimic mixture at a phospholipid concentration of 1mM (**dashed black line**). The inset in the upper right is a close-up of the phase transition. ***Middle Panel*****:** Denaturation profiles of 13 μM human Syt I C2A (residues 96-265) in the presence of 1 mM LUVs (unless stated otherwise) of different lipid compositions and 1mM Ca^{2+}. **solid black line** represents the denaturation with POPC:POPS (60:40); **blue dashed and dotted line** represents the denaturation with (POPC:POPS):cholesterol (80:20):30; **yellow dashed and dotted line** represents denaturation with the membrane domain forming lipid mixture from ***Table 3.1***; the **red dashed line** represents the denaturation with the membrane domain forming lipid mixture as SUVs; and **green dotted line** represents the denaturation with the SV mimic from ***Table 4.1***. All DSC scans were conducted in a buffer composed of 20mM MOPS and 100mM KCl at a pH of 7.5. ***Right Panel*****:** FLT denaturation of C2AB fragment of Syt I in the presence of membrane with or without Ca^{2+}. **Red:** 0.75μM C2AB, 5.1mM Ca^{2+}, 110μM LUVs (60:40, POPC:POPS). **Orange:** 0.9μM C2AB, 600μM Ca^{2+}, 1.2mM LUVs (60:40, POPC:POPS). **Green:** 0.75μM C2AB, 110μM LUVs (60:40, POPC:POPS), 500μM EGTA. **Blue:** 0.75μM C2AB, 210μM LUVs (95:5, POPC:PIP2), 500μM EGTA. **Purple:** 0.75μM C2AB, 5.1mM Ca^{2+}, 210μM LUVs (95:5, POPC:PIP2). Right panel adapted from [18].

Figure 3.4: Change in the percent efflux of carboxyfluorescein from 200μM LUVs composed of a SV mimic lipid mixture (bottom) and LUVs composed of domain forming lipid mixture (top) injected with Ca^{2+} at 15 min and human Syt C2A domain (residues 96-265) at 30 min to final concentrations of 3mM and 13.33μM respectively. Δ%Efflux was calculated by subtracting control titrations in which no protein was added during the second injection. Arrows indicate the addition of Ca^{2+} (1^{st} injection), or protein (2^{nd} injection) during the course of equilibration. For titration controls in which Ca^{2+} or

protein were not present the injections were made with buffer composed of 20mM MOPS, 100mM KCl, 0.02% NaN_3, pH of 7.5. For all titrations the temperature was held constant at 20.4C until equilibration of the second injection when it was set to increase to 75˚C. The green line represents the temperature change over time, while the blue and purple dashed lines represent the temperatures (and corresponding titration times) at which the membrane phase transition occurs (purple) and the bound-protein denatures (blue). The efflux conditions for both plots were as follows: the **black solid line** represents the Δ%efflux in the presence of both the human Syt I C2A (residues 96-265) and Ca^{2+}, and the **red solid line** represents the Δ%efflux of the domain in the absence of Ca^{2+}.

Figure 4.1: CF release assay of 200μM CF containing liposomes at 200nm LUV diameter. αS containing samples contain 0.8μM peptide and 200μM CF containing liposomes. Unbound αS and bound αS containing samples were run from 40°C to 0°C through the phospholipid bilayer transition temperature calculated to be approximately 27°C. 38:38:24 POPE:SOPE:POPS liposomes in the presence (**green**) and absence (**black**) of αS (**left panel**); and (38:38:24):45 (POPE:SOPE:POPS):Cholesterol in the presence (**green**) and absence (**black**) of αS (**right panel**). Time to temperature conversion is plotted and inset on **right panel**.

Figure 4.2: Heating thermograms of 38:38:24 POPE:SOPE:POPS LUVs (left) and SUVs (right) in the presence (**red**) and absence (**black**) of bound αS. All scans were conducted at a phospholipid concentration of 10mM, in 20mM MOPS, 100mM KCl, pH 7.5 buffer. Upon addition of αS to the LUV mixture, corrections in molar phospholipid concentration were accounted for. Scans are normalized to the appropriate phospholipid concentration in each case.

Figure 4.3: CD spectra from thermal denaturation of αS in the presence of different liposome mixtures and curvature sizes. Thermal denaturation observed from 37°C to 91°C. A) 15μM αS in the presence of LUVs (60:40 POPC:POPS) at a 250:1 [L]:[P] ratio, where strongest α-helical structure observed at 37°C; B) 15μM αS in the presence of SUVs (60:40 POPC:POPS) at a 375:1 [L]:[P] ratio, where strongest α-helical structure observed at 37°C; C) 5μM αS in the presence of synaptic vesicle mimicked SUVs at a 200:1 [L]:[P] ratio, where secondary structure determination is unclear.

Figure 4.4: Average of three CD spectra at 37°C, 39°C and 41°C where the strongest helical content was observed, of 15μM αS in the presence of LUVs (**black**) at a 250:1 [L]:[P] ratio, and SUVs (**red**) at a 375:1 [L]:[P] ratio. LUVs and SUVs were of a 60:40 POPC:POPS phospholipid mixture.

Figure 4.5: Heating thermogram of 20μM αS in the presence of synaptic vesicle mimicked SUVs at a 200:1 [L]:[P] ratio from 35-90°C. Raw data represented as **black circles**, and model fit line represented as **black solid line**.

Figure 4.6: Free energy stability plot of αS in the presence of SV mimicked SUVs. Stabilities were calculated using the Gibbs-Helmholtz equation, utilizing ΔH, ΔCp and Tm obtained from the DSC thermal denaturation profile.

Abbreviations:

Met:	Methionine
DSC:	Differential Scanning Calorimetry
CD:	Circular Dichroism
SV:	Synaptic Vesicle
αS:	α-Synuclein
CF:	Carboxyfluorescein
DMC:	Double Mutant Cycle
Ala:	Alanine
TFE:	Tetrafluoroethylene
NMP:	1-Methyl-2-Pyrrolidinone
TFA:	Trifluoroacetic Acid
HPLC:	High-Performance Liquid Chromotography
MS:	Mass Spectrometry
YM:	Tyrosine-Methionine
YM (ox):	Tyrosine-Methionine (oxidized)
FM:	Phenylalanine-Methionine
FM (ox):	Phenylalanine-Methionine (oxidized)
YA:	Tyrosine-Alanine
FA:	Phenylalanine-Alanine
AM:	Alanine-Methionine
AM (ox):	Alanine-Methionine (oxidized)
AA:	Alanine-Alanine
Syt I:	Synaptotagmin I
Dys:	Dysferlin
TF:	Tryptophan Fluorescence
PM:	Plasma Membrane
PS:	Phosphatidylserine
PC:	Phosphatidylcholine
PI:	Phosphatidylinostitol
PE:	Phosphatidylethanolamine
SM:	Sphingomyelin
POPC:	1-Palmitoyl-2-Oleoyl-*sn*-Glycero-3-Phosphocholine
POPS:	1-Palmitoyl-2-Oleoyl-*sn*-Glycero-3-Phosphoserine
POPE:	1-Palmitoyl-2-Oleoyl-*sn*-Glycero-3-Phosphoethanolamine
SOPE:	1-Stearoyl-2-Oleoyl-*sn*-Glycero-3-Phosphoethanolamine
LUV:	Large Unilamellar Vesicle
SUV:	Small Unilamellar Vesicle

Chapter One: Introduction to structural dependence on internal sequence and binding partners

1.1 Introduction and Background

A protein or peptide's structure is dependent on the internal interactions between the amino acid residues, or external interactions with the environment. Internal interactions can result from amino acid characteristics, such as side chain size, hydrophobicity or charge. These interactions dictate secondary structural character of the protein resulting in α-helical or β-sheet folded states or an unfolded, randomly coiled state. The influence of oxidation of a Met residue in aromatic-Met α-helix interactions was studied. Through oxidation of the Met side chain structural stability of the folded or ordered complex is altered, as a direct representation of side chain interaction roles in protein folding.

The resulting folded or unfolded state of the protein dictated by its internal sequence can further be affected by the characteristics of ligand binding. Ligand binding of the protein to a small molecule or a membrane surface can induce structural changes in folded conformation or strength of the folded state due to the necessary function of the protein. Proteins that lack strong internal interactions contributing to their structural specificity in a non-ligand bound state, classify as an intrinsically disordered protein, resulting in a randomly coiled, unfolded solution state. This randomly coiled state of the protein is the disordered, unstructured state, obtained prior to binding or induction of secondary external interactions. Ligand binding partners of intrinsically disordered proteins are initiators of secondary structure formation of the complex, making these proteins difficult to study in the absence of ligand. The effect of membrane composition and/or curvature was used to study the structural and functional effects of multiple intrinsically disordered membrane binding proteins. Induced changes in structural conformers of these proteins is dependent on binding specificity and membrane order, leading to advances in understanding

their functional and mechanistic properties. These proteins, found in the neuronal environment were observed as their obtained structured conformers when binding specific ligands and/or ranges of complex physiological lipid membrane surfaces are impacted.

The induced structural state of specific peptides or proteins due to internal sequence features and binding partners is presented here to assist in determining the function and significance of specific complexes. By understanding the changes that occur within protein structure due to internal and external interactions, the interactive properties of the specific complex can be more defined.

Chapter Two: Oxidation increases the strength of the methionine-aromatic interaction

2.1 Double mutant cycle significance and introduction

Through recent computational studies, it has been hypothesized and observed that an aromatic-Met interaction increases the structural stability of an ordered or folded protein upon oxidation of the Met side chain. Aromatic-Met interactions are present in ~33% of protein structures (2012, Protein Data Base), where the majority of these sequences have more than five instances of this interaction occurring. This interaction of oxidized Met and aromatic is significantly stronger than a hydrophobic interaction, indicating it could play a role in stabilizing the protein's structure, but also in ligand-binding [1]. Through protein sequence/structure analysis, aromatic-Met interactions are abundant when compared to non-sulfur-aromatic interactions [2]. Met's sulfur group is important, due to its propensity to form interactions with aromatic side chains within α-helical structures at *i* and *i* + 4 positions [3]. Met's susceptibility to sulfur oxidation allows this study to become significantly important to a wide range of diseases including Crohn's Disease [4], irritable bowel syndrome [5], pulmonary fibrosis [6, 7, 8], cancer [9,10] and many others.

A helix/coil approach [3] was used to experimentally study this interaction via DSC and CD, where the calculated enthalpy, or strength of stability of the ordered state, increases for two aromatic-Met induced peptides upon Met oxidation. An experimental energetic evaluation of the strength of interaction between an aromatic and Met residue corroborate computational findings of an oxidized Met construct as more stable than its un-oxidized form. As a means of eliminating the possibility of potentially unknown additional contributing interactions within the 15-mer constructs, a double mutant cycle (DMC) was constructed [11, 12, 13]. A DMC experiment enables evaluation of the contribution of specific residues to a peptide's structural stability.

To construct a DMC, peptide constructs where each of the key residues, in this case aromatic residues and Met, were systematically replaced by the neutral residue alanine (Ala) at singly and then doubly, where Ala replaces one or both residues respectively. By evaluating the difference in ΔG between the Met-aromatic (oxidized or un-oxidized) and its respective singly substituted construct, giving a ΔΔG and then subtracting the ΔΔG of the singly substituted to the doubly substituted mutant, the result is a $\Delta\Delta\Delta G_{Int}$ (***Figure 2.1***). The value of $\Delta\Delta\Delta G_{Int}$ indicates if the specific interaction is contributing to the stabilization of structure. If $\Delta\Delta\Delta G_{Int}$ equals zero, the interaction observed is not contributing to the structural stability, if greater than zero, the interaction is stabilizing and if less than zero, destabilizing [11, 12, 13].

2.2 Materials and Methods

Peptide Synthesis

To study the appropriate pair sequences in a peptide chain, the un-oxidized amino acid Met and oxidized Met (ox) was inserted into the sequence: a) Tyr-Gly-Gly-Ser-Ala-Ala-Glu-Ala-***Aromatic***-Ala-Lys-Ala-**Met**-Ala-Arg-NH2, b) Tyr-Gly-Gly-Ser-Ala-Ala-Glu-Ala-***Aromatic***-Ala-Lys-Ala-**Met (ox)**-Ala-Arg-NH2. The design of those peptides, a capping box at the N-terminus and blocked at the C-terminus, is based on [3]. The peptides were assembled on Fmoc-PAL-PEG-PS resin by Fmoc

chemistry using a PE Biosystems PioneerTM protein synthesis system. Single Met oxidation was accomplished by incorporation of Fmoc-Met (ox)-OH during synthesis. Standard *N*-[(dimethylamino)-1*H*-1,2,3-triazolo[4,5-*b*]pyridin-1-ylmethylene]-*N*-methylmethanaminium hexafluorophosphate N-oxide (HATU)/ *N,N*-diisopropylethylamine (DIEA) (1/2.4 eq.) activation, in 1-methyl-2-pyrrolidinone (NMP), was applied. Fmoc deprotection was achieved with 20% piperidine in NMP. The final release of the peptides, with removal of the side chain protecting groups, were accomplished by exposure of the peptide-resin to 82.5% trifluoroacetic acid (TFA), 5% phenol, 5% thioanisol, 2.5% 1,2-ethanedithiol, 5% water (Reagent K). The peptides were precipitated with cold methyl-*t*-butyl ether, vortexed, centrifuged, decanted, and dried over argon. The dried peptide was dissolved in degassed water and purified by high-performance liquid chromatography (HPLC) using a reversed-phase C8 HPLC column. Peptide elution was achieved with a linear gradient from 0 to 34% B (95% acetonitrile / 5% water / 0.1% TFA) in 40 min at a flow rate of 2.5 mL/min with detection at 280 nm using a System Gold Beckman Coulter system. The HPLC fractions were collected and analyzed by mass spectrometry (MS).

Circular Dichroism Spectroscopy (*Peptide Studies*)

All peptides were stored in tetrafluoroethylene (TFE) post synthesis, the organic solvent was removed via evaporation using N_2 gas prior to use. To ensure complete removal of the TFE, the sample was then put under vacuum for one hour. The dried peptide was re-constituted in 10mM KH_2PO_4, 100mM KCl at pH 7.5, and prepared for CD data collection. All CD experiments were performed on a Jasco J-815 CD Specrometer (Annapolis, MD) using a 0.1cm quartz cuvette using 150μM peptide concentration for all samples. Concentrations of the peptide samples were determined using a Nanodrop Spectrometer. Data points were collected from 200 to 260nm in 1nm increments from -2°C to 60°C for YM, YM (ox), FM and FM (ox). Peptides used for the DMC, YA, FA, AM, AM (ox) and AA, one data point was collected at 222nm at each 0.5°C or 2°C change as temperature increased from -2°C to 60°C. Cooling melts were also collected on all peptides (YM, YM (ox), FM,

FM (ox), YA, FA, AM, AM (ox), AA) similar to the DMC, as temperature decreased from 60°C to -2°C. All collected data points were an average of 3 acquisitions of the ellipticity recorded.

Differential Scanning Calorimetry (*YM and YM (ox)***)**

All peptides were stored in TFE post synthesis; the organic solvent was removed via evaporation using Ar gas prior to use. The dried peptide was then re-constituted in 10mM KH_2PO_4, 100mM KCl at pH 7.5, and prepared for DSC data collection. DSC experiments were performed on a NanoDSC (TA Instruments, New Castle, DE) at a scan rate of 1°C/min. DSC experiments were conducted at 100μM peptide concentration for un-oxidized, and 150μM for oxidized. Concentrations of the peptide samples were determined using a Nanodrop Spectrometer. To ensure the enthalpy measured was independent of concentration, experiments were conducted at different concentrations.

2.3 Double mutant cycle results

Utilization of the DMC is dependent on evaluation of the free energy (ΔG) of the ordered to disordered transitions of the nine peptide constructs (***Table 2.1***). CD directly measured the change in ellipticity as a function of temperature to analyze thermal melting and cooling of each construct. Based upon the observation of: 1) an isodichroic point in each of the peptide constructs and [14] 2) reversibility in the change in ellipticity of each peptide construct, defined by heating and cooling melt overlap, free energies were calculated through the use of a two state (ordered to disordered) model.

A common elliptic value at ~202nm upon changing temperature was observed upon spectra overlay (***Figure 2.2***). This isodichroic point is indicative of two state behavior [14]. The spectra at the lowest temperature are consistent with the presence of α-helical (ordered) content that upon increasing temperature, the structure transitions to a more randomly coiled (disordered) state.

Heating and cooling melts of four aromatic-methionine peptides (YM, YM (ox), FM, FM (ox)) (***Figure 2.3***) show absence of hysteresis indicating reversibility. Lack of hysteresis is also shown in the five mutated peptides (YA, FA, AM, AM (ox), AA) used in determining $\Delta\Delta\Delta G_{Int}$ (***Figure 2.4***).

Based upon the determination of a two state compliance through isodichroic and heating/cooling melt overlap, thermodynamic analysis was undertaken on all nine constructs. The Gibbs-Helmholtz equation was used to relate the free energy to the change in temperature, which is dependent upon the enthalpy (ΔH_{Tm}), change in heat capacity (ΔCp), and transition temperature (Tm). As such, the enthalpy change (ΔH_{Tm}) associated with this process at the transition temperature is a parameter from the global fit of the fractional change of signal with temperature. Fit parameters (enthalpy change, transition temperature, and heat capacity change) for YM and YM (ox) were tested by comparing the parameters obtained via the fit of the CD data to the same parameters directly measured by DSC. DSC monitors the rate of change of heat absorbed with increasing temperature (Cp), integration of this signal change with temperature is enthalpy (ΔH_{Tm}). The transition temperature (Tm) is the midpoint of the area of the curve, and the change in heat capacity (ΔCp) is the difference in the pre and post transition baselines.

The denaturation data was fit using a two state assumption, where the peptide transitions from a structured to unstructured state. From this assumption the K, or equilibrium constant, of this transition is equal to concentration of the unfolded peptide divided by the concentration of the folded peptide:

$$K = \frac{[U]}{[F]} \qquad \text{(Equation 2.1)}$$

To further test the validity of this assumption, the enthalpy associated with a two

state transition (Van't Hoff enthalpy) was calculated from the CD data using the equation $\Delta H_{VH}=4RTm^2\ (d\Theta/dT)_{Tm}$ where R is the ideal gas constant, Tm is the transition temperature, Θ is the normalized ellipticity at 222nm, which is the fractional change in the states, and $(d\Theta/dT)_{Tm}$ is the slope at the mid-point of the transition, then compared to the enthalpy change obtained through fitting the data. The closer the values of the enthalpies of the fit and the Van't Hoff are to one another, the more compliant the transition is with two-state behavior and the closer the ratio of the enthalpies is to one. The oxidized and unoxidized constructs had ratios of 0.86 and 0.85 respectively, consistent with a transition from a structured to unstructured state. Along with this the Van't Hoff ratio was also calculated for the enthalpy determined through DSC for both, YM and YM (ox) peptide constructs according to $\Delta H_{VH}=4RTm^2(\Delta Cp_{Max}/\Delta H_{cal})$, where ΔCp_{Max} is the maximum of the endotherm, and ΔH_{cal} is the enthalpy found through the DSC. This gave a Van't Hoff ratio of 0.83 and 0.63 for the unoxidized and oxidized constructs respectively, consistent with two state behavior. Note these enthalpies are at the detection limit of DSC, and there is more noise associated with the endotherms than the CD data. The ΔH_{Tm} value was further confirmed by comparing the enthalpy from the fit of the CD data to the enthalpy directly measured via DSC for both peptide constructs (***Table 2.2***).

Conformity of thermodynamic analysis with physical reality was evaluated through direct comparison of the melting transition temperatures. The melting transition temperature in a two state model occurs where the population of folded peptide equals the population of unfolded peptide or where each is occupying 0.5 of the population (***Figure 2.5***). A fraction of unfolded peptide indicated as α or $F_{Unfolded}$, represents the fraction unfolded at any temperature in the melting range:

$$F_{Unfolded} = \alpha = \frac{[U]}{[U]+[F]} \qquad \text{(Equation 2.2)}$$

Fraction unfolded is represented as concentrations, and can be converted to an equation of the signal observed for each peptide unfolded (disordered)→folded (ordered) transition. A representation of fraction unfolded in terms of ellipticity, or Θ:

$$\alpha = \frac{\Theta_{Total} - \Theta_{Folded}}{\Theta_{Unfolded} - \Theta_{Folded}} \qquad \text{(Equation 2.3)}$$

Where Θ_{Total} is the observed ellipticity at each temperature, Θ_{Folded} is the ellipticity of the fully ordered form of the peptide and $\Theta_{Unfolded}$ is the ellipticity of the fully disordered form of the peptide. The convergence of fit values of the transition temperature with the plotted midpoint of the CD thermal denaturation curves strongly indicates the correlation of the fit parameters.

Thermodynamic parameters necessary to complete a DMC were determined through this thermodynamic analysis, displayed in ***Table 2.3*** and ***Table 2.4***. All peptides were fit as described above, using the Gibbs Helmholtz equation, giving $\Delta H_{Tm,\ CD}$ (kcal/mol), ΔCp (kcal/molK) and Tm (°C) values. The aromatic-Met peptides are displayed in ***Table 2.3***, and peptides used for $\Delta\Delta\Delta G_{Int}$ analysis are displayed in ***Table 2.4***.

In $\Delta\Delta\Delta G_{Int}$ determination, the difference in ΔG of the mutated aromatic in the presence and absence of methionine from the wild type results in the $\Delta\Delta G_{AroM \rightarrow AlaM}$ and $\Delta\Delta G_{AroAla \rightarrow AlaAla}$:

$$\Delta\Delta G_{AroM \rightarrow AlaM} = \Delta G_{AroM} - \Delta G_{AlaM} \qquad \text{(Equation 2.4)}$$

$$\Delta\Delta G_{AroAla \rightarrow AlaAla} = \Delta G_{AroAla} - \Delta G_{AlaAla} \qquad \text{(Equation 2.5)}$$

The difference of these two ΔΔG values gives a ΔΔΔG of interaction correlating to the observed residue interaction contributing to structural stability or de-stability:

$$\Delta\Delta\Delta G_{Int} = \Delta\Delta G_{AroM \rightarrow AlaM} - \Delta\Delta G_{AroAla \rightarrow AlaAla} \qquad \text{(Equation 2.6)}$$

The $\Delta\Delta\Delta G_{Int}$ indicates that other interactions contributing to structure have been removed from the observation allowing for determination of the free energy contributing toward an ordered state of the peptide due to the aromatic-Met interaction [11, 12, 13]. It can be seen in ***Table 2.5*** that the ordered stability contribution of the oxidized state of each aromatic-Met peptide is ~0.4/0.6 kcal/mol greater than that of the un-oxidized form of the peptide. This increase in free energy seen in the calculation of $\Delta\Delta\Delta G_{Int}$ indicates the oxidized Met residue is causing an increase in ordered stability of these peptides.

Although the CD thermal denaturation curves are fit using the Gibbs Helmholtz two state transition, it is important to address the lack of limiting baseline behavior at the completely ordered state of the peptide. At -2°C a completely ordered limiting value, or slope equal to zero, is not obtained which indicates a fully ordered state was not achieved. Observation of the full peptide's transition was observed using DSC for YM and YM (ox) peptides (***Figure 2.6***) which indicates completely ordered behavior is reached at 0°C. Due to the high concentration and larger volume needed for DSC experiments, CD was used for thermodynamic analysis of FM, FM (ox) and all five DMC constructs. The comparison and consistency of fit DSC and CD data for the original YM and YM (ox) peptides, indicates the strength of this thermodynamic analysis. The analysis proposed is consistent with the hypothesis in that an increase in structural strength and stability is caused from the oxidation of Met in the aromatic-Met interaction. By computing DMC free energies of interaction, there remains a consistent relationship of each peptide contribution, giving strength to the significance of these values. The DMC relationship is consistently in agreement with the experimental analysis of increasing strength due to oxidation and should not be disregarded. Through two state certainty via an isodichroic point and overlay of heating and cooling melts, these peptide constructs accurately depict two state

behavior. Further analysis should be completed through DSC to clarify the fully ordered states of these peptides, giving clarity to the lack of limiting baseline behavior at low temperatures.

Chapter Three: Randomly organized lipids and marginally stable proteins: a coupling of weak interactions to optimize membrane signaling

3.1 Introduction

A cell membrane is a pliable and responsive surface. Changes in the local environment of a given lipid are propagated in all directions within a leaflet by the weak cooperative interactions between each lipid molecule and its six nearest neighbors [15]. This type of propagation behavior suggests that the membrane has great signaling potential. Another key facet to consider with regard to biological membranes and signaling is the high degree of lipid species diversity. The distribution and diversity of lipids in eukaryotic membranes is thought to maintain the system in a nearly random distribution which, according to information theory [16], maximizes the amount of information that can be cooperatively propagated in a signaling event because it is not biased in any one direction as in a more ordered system. Together, the weak cooperativity of lipid molecules and their nearly random distribution suggest the membrane constitutes a major information transducer in the cell.

To transduce the vast array of information encoded within the mosaic membrane into the cell interior requires both transient organization of the signaling lipid species and a recipient protein that further senses and propagates the message. A lipid mixture near a critical point, teetering on a phase boundary between random distribution and restricted domain, could fulfill the first requirement. Domain formation can increase the probability of a particular signaling event, for instance, by

providing platforms for protein-protein interactions that initiate the intracellular portion of a signaling cascade. In this sense, transient order in lipid organization allows for a discrete message to be propagated at levels above background thermal noise, or in other words, above the milieu of all other possible messages encoded in the membrane lipid distribution.

Subsequent detection and propagation of such a wide range of membrane-encoded messages would seem to require a protein with complementary features; the protein would need to have a tendency towards random distributions so as to maximize the amount and diversity of information that can be recognized and propagated. Intrinsically disordered proteins are one well-known class of proteins with this tendency. Intrinsically disordered proteins are natively unfolded and have significant structural and conformational plasticity making them uniquely sensitive to differences in local environment, not unlike the near random but pliable membrane surface. Moreover, intrinsic disorder can facilitate propagation of information within the body of a protein [17]. When we measured the stability of a specific class of proteins by thermal denaturation we found that these proteins, whose functional role is directly linked to membrane biology, have features of intrinsic disorder; these proteins retain some secondary structure, but are marginally stable or nearly disordered [18, 19, 20]. Specifically, this seems to be the case with C2 domains of synaptotagmin I (Syt I) in neurons (involved in exocytosis) and the C2 domains of dysferlin (Dys) in muscle (responsible for sensing and repairing membrane damage). Currently, there are 14496 C2 domains annotated in 9258 protein sequences within the SMART non-redundant database [21]. It is unknown if this marginally stable behavior is a general feature of C2 domains, but denaturations carried out previously on various C2 domains from protein kinase C also converge on this finding [22]. Moreover, when we denatured the C2A domain of cotton Syt I, we found it had the same hallmarks as human Syt I, suggesting potential conservation across phylogenetic kingdoms.

A new potential rule for membrane signaling emerges when we simultaneously consider the near disordered nature of membrane lipids as well as membrane-sensing proteins, namely maximum flow of signaling information through the membrane and into the cell is optimized by the cooperation of the two near-random distributions of membrane lipids and proteins. Indeed, when lipid species diversity and protein intrinsic disorder are compared, both increase with organism complexity [23, 24]. While at first glance, this hypothesis may seem to imply uni-directionality of information flow (a marginally stable protein only decodes the information of the membrane), the mechanism applies in both directions. Protein interactions with membranes can induce membrane domain formation (order) if the protein has specificity for some of the lipids and these lipids are distributed non-ideally [25, 26]. If, however, the protein's interaction with the membrane depends on intracellular signals (such as calcium ion), then the protein becomes a means to relay intracellular conditions back to the membrane potentially for amplification via weak cooperative lipid-lipid interactions. The end result is reciprocal exchange of information.

Here we explore our hypothesis that the distribution of lipids within the eukaryotic membrane is coupled to interactions with weakly stable but structured proteins to transduce and modulate signaling information. Studies of protein stability and membrane disruption were completed in which membrane lipid composition is a variable. C2 domain stabilities are found to be highly sensitive to changes in lipid composition and undergo correlated changes with membrane information content.

3.2 Materials and Methods

Protein Constructs

The C2 domains studied were constructs derived from human Syt I, cotton Syt I, and Dys. The only C2A construct of human Syt I used for experiments in this study, contained residues 96-265. In the top half of ***Table 3.1***, thermodynamic parameters

are reported for a shorter human Syt I C2A construct containing residues 140-265. Additional residues in the 96-265 C2A construct correspond to the region between C2A and Syt I's single transmembrane helix. The human Syt I C2B domain included residues 272-422. The constructs from Dys include two different isoforms of the C2A domain: the canonical C2A domain (C2A wild type/C2A) and the variant resulting from alternative splicing of the first exon (C2Av1). Of the two C2 domains in cotton Syt I, only the C2A domain was studied. Purification of these constructs was carried out as previously described [18, 19, 20].

Preparation of Lipid Samples

All lipids were purchased from Avanti Polar Lipids (Birmingham, AL). Samples without cholesterol were prepared as previously described [20]. Cholesterol-containing samples were prepared by aliquoting lipid stocks into a 4:1 mixture of chloroform:methanol followed by rotary evaporation using a Buchi R-215 at a temperature between 50-60°C. The lipid films were then placed under vacuum for a minimum of 8 hours to remove excess solvent and hydrated with the appropriate buffer. LUVs were prepared by hand extrusion using a 0.1μm filter. SUVs were prepared through multiple rounds of extrusion with filters of gradually smaller pore sizes ending with a 0.03μm pore size.

Differential Scanning Calorimetry (DSC)

DSC experiments as well as both scan rate and concentration dependent controls were performed on a NanoDSC (TA Instruments, New Castle, DE) as described previously [18, 19, 20]. All scans were conducted in chelexed 20 mM MOPS, 100 mM KCl, pH 7.5 using saturating ligand concentrations. All scans with lipid contained one of the following: 1) LUVs of 60:40 POPC:POPS; 2) LUVs of (80:20):30 (POPC:POPS):cholesterol; 30 mole percent cholesterol was doped on top of a mixture POPC:POPS (80:20) 3) LUVs with the mixture shown in ***Table 3.2*** plus 45 mole percent cholesterol doped in; or 4) SUVs of 3). The concentration of the calcium stock solution used for all scans was verified using both a calcium ion

selective electrode (ThermoScientific) and a BAPTA chelating assay (Invitrogen/Molecular Probes, Eugene, OR). The concentration of all lipid stock solutions was confirmed through a phosphate assay according to standard protocols [20]. For the experiments reported in this study the human Syt I C2A construct was found have an average reversibility of 93% except in the presence of LUVs composed of the membrane domain forming mixture in which the reversibility was found to be 46%. For a justification of the thermodynamic parameters reported for the other domains discussed please see references [18, 19, 20].

Tryptophan Fluorescence

Tryptophan Fluorescence (TF) experiments were performed on a Lifetime Spectrometer (Fluorescence Innovations, Bozeman, MT) using nanomolar protein concentrations as previously described [18, 20]. No time-resolved measurements were made; instead the integrated intensity of the lifetime decay was used to monitor intrinsic tryptophan fluorescence (excitation and emission wavelengths of 295 and 340 nm, respectively). Buffers, Ca^{2+} stocks, and lipid samples used were identical to that described above. Percent reversibility was measured by comparing the integrated fluorescence lifetime intensity of the sample before heating and after cooling. Due to the exceptionally low stability of the Dys and cotton Syt I C2A domain, no change in tryptophan fluorescence could be detected for these constructs. As a result, only the Syt I C2 domains were studied using this method.

Circular Dichroism Spectroscopy

CD experiments were performed on a Jasco CD Spectrometer (Annapolis, MD), using 15μM of the Syt. I C2A domain (residues 96-265) with 700μM LUVs composed of POPC:POPS (60:40) and 1mM Ca^{2+} in a 0.1 cm quartz cuvette. The spectrum was obtained in the same buffer system used for DSC and TF. Data points were collected in 1 nm increments and averaged over 5 acquisitions. Spectra collected were corrected for any buffer contributions by subtracting a buffer scan from the corresponding protein scan.

Carboxyfluorescein Release Assay

LUVs containing CF dye were prepared as previously described [21]. To determine the effect of protein binding on membrane leakage, the dye signal was monitored with excitation and emission wavelengths of 492 nm and 515 nm, respectively, as a function of time and temperature, with one addition of ligand and one addition of protein. In the absence of ligand or protein, 20mM MOPS, 100mM KCl, 0.02% NaN_3 was added to obtain constant increases of volume at each addition of solution. All fluorescence measurements were performed on a Fluorolog 3 double excitation and double emission monochromoter (Horiba Jobin Yvon) in a 500μL quartz cuvette. Appropriate temperatures were chosen to enhance membrane transition and perturbation of the LUV lipid compositions listed in ***Table 3.2***, on which the experiments were performed [27]. Time and temperature dependent experiments were performed for a period of 60 minutes using a temperature controlled water bath (Pharmacia Biotech Multitemp III). The cuvette contained 300μL of liposome sample at the start of the fluorescence scan, 100μL of buffer or Ca^{2+} solution titrated in after 15 minutes, and 85μL of buffer or protein titrated in after 30 minutes. The cuvette was placed in the fluorometer and the scan was immediately started at constant temperature (20.4°C). Buffer or Ca^{2+} solution was added at 15 minutes, followed by buffer or protein at 30 minutes. At the time of the second injection, the temperature was set to increase to 75°C and the change in CF fluorescence was monitored in order to confirm consistency between experiments as well as dye release. Within the cuvette the concentration of liposome was 200μM and concentration of Ca^{2+} ion solution was 3mM after its addition at 15 minutes. A 50.6μM stock sample of the Syt I C2A domain (encoding residues 96-265) was added in one increment of 85μL to obtain a concentration of 13.33μM. Triton X-100 detergent was added after each scan to completely disrupt the membrane and confirm the presence of CF within the liposome as well as determine the maximum efflux.

3.4 Results and Discussion

C2 domains at neuronal, muscle, and plant membranes are weakly held together

C2 domains are functional modules exploited by numerous proteins in membrane trafficking and signaling events [28, 29]. As such, they are likely candidates for the decoding and propagation of information stored within the membrane's changing lipid distribution. Currently, there are 39 unique crystal structures of C2 domains that have been assigned via SCOP classification [29]. Of these structures most share a similar overall fold such as those in human Syt I, the canonical and variant forms of Dys, cytosolic phospholipase A_2 α, protein kinase C, and extended synaptotagmins (***Fig. 3.1***) [19, 28, 29, 30]. No crystal structure is available for *Gossypium* (cotton) Syt I; however, a good quality homology model can be computed based on its similarity with human Syt I. While the C2 domain structures of human and cotton Syt I as well as the canonical and variant forms of Dys C2A are highly similar, their free energies of stability at 37 °C ($\Delta G_{37°C}$) are not, spanning from 0.017-2.32 kcal/mol (***Fig. 3.2, lower panels; Table 3.1***). Despite this range, these different C2 domain stabilities are similar in the sense that all are at the lower limit of what constitutes a folded protein and all have features of protein disorder. Given that marginal stability is found in C2 domains from tissues of different embryonic origin (neurons and muscle) as well as different eukaryotic organisms (humans and plants), it brings up the question of whether or not this is a conversed feature of membrane associated C2 domains. The initial data presented here suggests this may be the case and earlier DSC denaturation work on the α-, β-, and γ-isoforms of protein kinase C, wherein all C2 domains were found to have a $\Delta G_{37°C}$ of ~1 kcal/mol, further supports this hypothesis [22].

Membrane composition and curvature set the protein ensemble

The marginal stability of the C2 domains tested above suggested that each would be sensitive to changes in their local environment, particularly the membrane surface with which they interact [31, 32]. To test this hypothesis, a C2 domain construct of

human Syt I was denatured in the presence of vesicles of varying lipid composition and the resulting data was used to calculate $\Delta G_{37°C}$. Human Syt I C2A (encoding residues 96-265) in the presence of non-domain forming LUVs (60:40 mixture of POPC:POPS, ***Fig. 3.3 upper left panel***) was found to be weakly stable with a $\Delta G_{37°C}$ of 2.18 kcal/mol (***Fig. 3.2, upper left panel; Table 3.1***). When the composition includes cholesterol ((80:20):30 mixture of (POPC:POPS):chol as LUVs), this basal stability decreases to 1.67 kcal/mole (***Fig. 3.3, middle panel; Table 3.1***).

When the LUV membrane complexity mimics the heterogeneity of the plasma membrane (PM) (***Table 3.2***), C2A's stability and unfolding profile undergo additional dramatic changes (***Fig. 3.3, middle panel***). This PM mimic is based upon the distribution and mole percents of lipid species found in a SV, specifically the cytosolic face with which Syt I interacts *in vivo* [33]. In the presence of this SV mimic and saturating Ca^{2+}, human Syt I C2A has a stability of 5.75 kcal/mol. If, however, physiological unsaturated PS and PI lipids are replaced with PS and PI containing saturated acyl chains, a chimeric lipid mixture is made; the composition of which still replicates the general characteristics and distributions found in a synaptic vesicle, but also weakly forms domains as suggested by the subtle DSC transition seen with LUVs alone (***Fig. 3.3, left panel***). Using this LUV chimera, the calculated $\Delta G_{37°C}$ in the presence saturating Ca^{2+} was 7.09 kcal/mol and increased further still to 7.6 kcal/mol using SUVs of identical composition. Indeed, human Syt I C2A's $\Delta G_{37°C}$ increases 23% (5.75 to 7.09 kcal/mol) in response to this local change in lipid distribution and increases an additional 7% (7.09 to 7.6 kcal/mole) in response to increased curvature. This latter observation is of particular importance to human Syt I because vesicles undergoing exocytosis and subsequent recycling experience a broad range of positive and negative curvatures both of which can change lipid distributions [34, 35]. If Syt I senses these changes, as suggested by the change in $\Delta G_{37°C}$ presented here, it will have ramifications on the protein's conformational ensemble.

The same rule of membrane composition sensitivity seen for C2A alone seems to extend to the C2AB fragment of human Syt I, which includes both C2 domains of the protein [18]. The C2A and C2B domains are stabilized by different lipid species, where C2A is stabilized by PS and C2B by PIP_2 [18]. Because one domain becomes destabilized when the other is stabilized, both C2 domain ensembles are set by interactions with either lipid type. This is best illustrated in the TF denaturations of C2AB which have a strong fluorescence contribution from the C2B core tryptophan (***Fig. 3.3, right panel***). In the presence of 60:40 POPC:POPS LUVs, C2A is stabilized and C2B is destabilized (green). However, addition of Ca^{2+} drives C2A into a PS-bound state which makes the destabilization of C2B more prominent (orange and red). In contrast, when C2AB is in the presence of 95:5 POPC:PIP_2 LUVs, C2B is stabilized and C2A is destabilized (blue). As with PS-containing membrane, Ca^{2+} accentuates this effect (purple). The denaturations reveal a strikingly broad range of stabilities that highlight the ability of the membrane to broaden or narrow the conformational ensemble of C2B within the C2AB fragment using the lipid binding ability of either domain.

The responsiveness of human Syt I C2 domains is further exemplified by a few peculiar changes in the baseline heat capacity (ΔCp) (***Fig. 3.2, top left panel***). C2A and C2B have a very large ΔCp under some membrane conditions. As can be seen in ***Table 3.1*** the large ΔCp values can have a dramatic effect on the calculated stability of the domain, as it narrows the temperature range over which the protein appears stable and consequently can give rise to a negative $\Delta G_{37°C}$. While we are not concluding that the C2A domain is unfolded under these conditions (indeed at 25 °C, a temperature well below the calculated cold denaturation threshold, C2A is still folded; ***Fig. 3.2 top right panel***), the changes in ΔCp provide another metric for the protein's sensitivity to the local membrane environment. Both C2 domains of human Syt I are known to have partial membrane insertion capabilities [36, 37]. Moreover, structural orientation modeling of C2 domains bound to PIP_2 suggests a fairly large

surface area of contact between protein and membrane [38]. Since one contribution to the change in baseline heat capacity is the change in solvation of the protein in native and denatured states, partial insertion into the 60:40 POPC:POPS (for C2A) or 95:5 POPC:PIP_2 (for C2B) membranes, or significant reduction in solvent accessibility due to surface adherence could alter solvation of the native C2 domain. If in the unfolded form of the protein, hydrophobic residues partially partitioned into the membrane, solvation could also be altered leading to a change in ΔC_p. This latter example, however, would result in a reduced ΔC_p because hydrophic residues would be protected from aqueous solution and not be surrounded by water cages that differentially absorb heat. Since this is the opposite of our data, the large ΔC_p's point instead to unique membrane modifications of the native state. Regardless of the root cause, the behavior of the C2 domain is membrane composition and condition-dependent.

Unique Syt I C2A conformers invoke distinct membrane-disruption responses in a synaptic vesicle mimic

From the cumulative denaturation studies above, it appears that these C2 domains (from human Syt I, in particular) are acutely sensitive to membrane environment and are capable of adopting numerous conformations. This intrinsic plasticity leads to a question similar to that discussed for membrane lipid diversity and encoded information. Just as different lipid-lipid pairs constitute different potential signals, so too should C2 domain conformers. In this context, noise comes from the breadth of the C2 domain's conformational ensemble (determined by the free energy of stability). The signal is a particular subset of conformers that are simultaneously selected from the ensemble and more heavily weighted by binding of ligand (such as membrane and Ca^{2+}). The resulting conformer subset mediates molecular events that fulfill a biological function of the C2 domain as a means to propagate the given signal [39].

To test this definition of function, we applied our recently developed CF efflux assay

to human Syt I C2A using vesicles that had either the domain forming or non-domain forming SV compositions listed in ***Table 3.2***. From human Syt I C2A's change in stability shown above, it appears that the membrane domain forming mixture selects a smaller set of conformers from the ensemble (as suggested by the 23% increase in $\Delta G_{37^{o}C}$ compared to non-domain forming mixture). When looking at the change in efflux as a function of time, the C2A conformers selected by the domain forming mixture reduce release. This can be seen by the downward inflection at ~37 °C (where the phase transition occurs). However, when the lipid mixture mimics the SV, the extent to which C2A limits efflux increases; the downward inflection has a larger magnitude. In both cases, however, when the sample temperature increases beyond the melting temperature of C2A, the rate of efflux increases dramatically. Thus, the distinct C2A conformers selected by each lipid mixture send unique signals back to the membrane, resulting in differential efflux outcomes that may relate to function (***Fig. 3.4***) [39].

3.5 Closing Comments

Eukaryotic lipids are numerous. If each lipid combination is regarded as a potential signal, the eukaryotic membrane becomes a repository of information, highly diversified by chemical variation in head group and acyl chain. These signals likely have specificity, suggested by both the unique lipid distributions found amongst compartments and leaflets as well as the numerous proteins that selectively bind to, partition into, or enzymatically target them. Within this context, a non-random distribution of lipids (like those found in membrane domains) could reduce information in a local region of the membrane. Membrane domains are non-ideal mixtures of lipids. As such, domains could have fewer potential combinations of lipids and consequently less information. In this scenario, predictable signaling outcomes come about from restricting available combinations of lipids either in a signaling domain or upon protein binding.

Much like the membrane, C2 domains that associate with or are tethered to the membrane also seem to be dominated by weak interactions. This marginal stability imparts these proteins with a membrane-responsive character, where the conformational distribution of the protein is set by the lipid composition and information content. This selection/restriction of the protein conformational ensemble by the membrane can be viewed as a decrease in the informational entropy of the protein, which in turn reciprocally affects the membrane (***Fig. 3.4***). If lipid diversity is a means to store information and weakly stable membrane-associated proteins conformationally respond to membrane composition (***Fig. 3.2 and Fig. 3.3***) while simultaneously affecting membrane distribution (***Fig. 3.4***), then these weak interactions provide a means for translating and transducing membrane-encoded information to downstream effector molecules whether they be proteins required for membrane repair (Dys) or for regulated release of neurotransmitter (human Syt I). In both cases, noise that manifests as non-functional combinations of lipids or non-functional protein conformers is unrecognized by the cell; the cell cannot make sense of the information presented in these non-signaling states. However, when a particular signal is to be transmitted, the near randomness of both lipid distribution and protein structure condense into a particular configuration associated with the signal allowing for its propagation.

Chapter Four: αS's thermodynamic properties of SV trafficking

4.1 Introduction

αS is a protein found in the neuronal environment, involved in the regulation of SV transport to the PM. αS is a small intrinsically disordered, membrane binding peptide that regulates SV trafficking. It is the overexpression or mutation of this peptide that correlates to the onset of Parkinson's Disease (PD) [40]. This peptides functionally specific binding process has not been extensively studied and is unclear, leading to minimal understanding of its role in PD. It is hypothesized that upon binding the

membrane surface, αS reduces SV membrane rigidity within the bilayer before it fuses with the PM of the neuron. By reducing membrane rigidity, the vesicle has a higher propensity for fusion with the PM surface, to then excrete neurotransmitter contents into the synaptic cleft. The binding of αS to a SV is dependent on both the very unusual phospholipid composition of a SV, and on its very small size. The complex phospholipid head-group moiety that is present in a SV is significant to its proper trafficking and fusion capabilities. To accurately study this binding event, it is essential to determine the lipid composition that most closely mimics the outer leaflet of the SV membrane, the surface with which αS interacts. The dependence of αS-membrane binding affinity on the specific phospholipid components of SVs and the change in structural conformation of αS, upon binding different membrane compositions, will dictate the proper changes of the peptide for function. As an initial approach to the study of αS, a physiological mixture of phospholipids within a SV was determined. A complex synaptic mixture of phospholipids and cholesterol is the surface to which αS binds. The curvature of the membrane binding surface is significant to SVs, as the vesicle is only 0.03 microns in diameter, a highly curved bilayer surface is created [33]. The extent of membrane surface curvature to which a peptide can bind to, will induce different curved intensities of the bound conformer, further altering its defined folded state. Through thermodynamic analysis, the study of the peptide-membrane binding interface will lead to a clearer representation of the peptides proper function. The effect of mixture complexity and liposomal surface curvature has been explored through preliminary CF release assays, DSC and CD spectroscopy experiments.

4.2 Materials and Methods

Preparation of Lipid Samples

All lipids were purchased from Avanti Polar Lipids (Birmingham, AL). Samples without cholesterol were prepared as previously described [27]. Cholesterol-containing samples were prepared by aliquoting lipid stocks into a 4:1 mixture of chloroform:methanol followed by rotary evaporation using a Buchi R-215 at a

temperature between 50-60°C. The lipid films were then placed under vacuum for a minimum of 8 hours to remove excess solvent and hydrated with the appropriate buffer. LUVs were prepared by hand extrusion using a 0.1μm filter or 0.2μm (CF). SUVs were prepared through multiple rounds of extrusion with filters of gradually smaller pore sizes ending with a 0.03μm pore size.

Carboxyfluorescein Release Assay

LUVs containing CF dye were prepared as previously described [27]. To determine the effect of protein binding on membrane leakage, the dye signal was monitored with excitation and emission wavelengths of 492nm and 515nm respectively as functions of time and temperature. All fluorescence measurements were performed on a Fluorolog 3 double excitation and double emission monochromator (Horiba Jobin Yvon) in a 500μL quartz cuvette. Appropriate temperatures were chosen to enhance membrane transition and perturbation of the LUV lipid compositions, on which the experiments were performed [33]. Experiments were performed for a period of 60 minutes using a temperature controlled water bath (Pharmacia Biotech Millitemp III). A buffer composed of 20mM MOPS, 100mM KCl and 0.02% NaN_3 was used, with 200μM LUVs and 0.8μM αS when in the presence of peptide. Triton X-100 detergent was added after each scan to completely disrupt the membrane and confirm the presence of CF within the liposome as well as determine the maximum efflux.

Differential Scanning Calorimetry (*Liposome Transition*)

Liposome transition DSC experiments were performed on a NanoDSC (TA Instruments, New Castle, DE) at a scan rate of 0.167°C/min. DSC samples were prepared using 10mM liposome concentration of LUVs or SUVs. The liposome sample was annealed, or allowed to reach an ordered equilibrium by transitioning through a temperature range of 5-55°C. Once properly annealed, αS was re-constituted in 20mM MOPS, 100mM KCl at pH 7.5, and added to the sample to reach a 250:1 [L]:[P] ratio. The DSC sample then contained 18μM αS and 6.67mM

liposome. Concentration of αS was determined using a Nanodrop Spectrometer. Liposome concentration was determined through a phosphate assay and was used to determine enthalpy per mole of liposome [20].

Circular Dichroism Spectroscopy (αS**):**

αS was re-constituted in 20mM MOPS, 100mM KCl at pH 7.5, and prepared for CD data collection. All CD experiments were performed on a Jasco J-815 CD Spectrometer (Annapolis, MD) using a 0.1cm quartz cuvette using 5-15μM αS concentrations, and 1-5.6mM liposome concentrations for all samples. Concentrations of the αS samples were determined using a Nanodrop Spectrometer. Data points were collected from 200 to 260nm in 1nm increments from -2°C to 60°C. All collected data points were an average of 3 acquisitions of the ellipticity recorded.

Differential Scanning Calorimetry (αS *Transition*):**

One DSC experiment was performed on a NanoDSC (TA Instruments, New Castle, DE) at a scan rate of 1°C/min. αS was re-constituted in 20mM MOPS, 100mM KCl at pH 7.5, and the DSC sample contained 20μM αS and 4mM SV mimicked liposome concentration as SUVs. Concentration of αS was determined using a Nanodrop Spectrometer.

4.3 Determination of physiological SV mimic

The SV is comprised of many transmembrane domain proteins and a complex mixture of phospholipids that make up the bilayer of this small liposome. As determined from MS, 50.4% of the synaptic membrane surface is made of phospholipids, including both the inner and outer leaflets of the membrane bilayer. Cholesterol is found in a high mole percent concentration of a 1:0.8 mole ratio of phospholipid:cholesterol. MS analysis showed that SVs contain PC, PE, PS, PI, SM, cholesterol and hexosylceramide [33]. A quantitatively accurate characterization of this complex mixture is necessary to properly mimic the physiological binding

surface of αS, and to allow the determination of the deleterious effects of the peptide. However, the specific, yet different, inner and outer leaflet lipid compositions are not known. This is critical information as αS binds to the outer, not inner leaflet. PC and SM phospholipids are found in the outer leaflet of the PM indicating that αS does not bind a membrane of this composition [24]. The fusion of a SV to the neuron's PM forces the SV outer leaflet to become the inner leaflet of the bilayer. This fusion of the vesicle from the inner leaflet of the PM indicates that the inner leaflet of the fusing SV is comprised of PC and SM, correlating to the outer leaflet of the PM. Therefore, in order to mimic the outer leaflet of the SV, a phospholipid mixture excluding PC and SM was created. This outer leaflet mimic is then comprised of PE, PS, PI and cholesterol, as shown in ***Table 4.1*** [42]. PE, PS, PI and cholesterol percentages were calculated from the MS analysis of the tail length contributions from each phospholipid head group. The degree of saturation within phospholipid tails was calculated by their percent contribution in the MS analysis [33].

In an approach to defining the membrane interactions within the SV bilayer upon binding of αS, experiments observing membrane characteristics were designed. The difference in each phospholipid head group within the bilayer is known to effect protein/peptide binding, and to more clearly determine the impact of specific phospholipid head groups on the peptide's binding rearrangement, a simpler physiological mixture was studied, shown in ***Table 4.2***. The SV mixture was simplified to contain only PE and PS phospholipids, allowing for the direct impact of the two most prevalent phospholipids within a SV's outer leaflet, on αS binding. 98% of the mimicked SV composition is comprised of PE and PS, both anionic and negatively charged head groups [33]. By simplifying this mixture, the impact of specific head-groups on the binding of αS becomes clearer. Through studying these two phospholipid head-groups interactions with αS, the focus of the experiments is on lipid ordering, which determines bilayer rigidity. Upon binding of a peptide to the membrane surface, a specific rearrangement of phospholipids is obtained, which

strongly dictates affinity. Using this simplified mixture, direct observation of protein-induced changes in membrane order are observed. By studying αS's interaction with this simplified membrane surface, the binding parameters of αS to the membrane, dependent on membrane head-group composition, will be defined. It is this observation of membrane ordering that will bring understanding to the relevance of such a complex mixture to the binding and fusion of SVs.

4.4 Results and Discussion: membrane reordering due to αS binding

The high content of cholesterol within the SV mimic and simplified SV mimic, lipid mixture is an important feature regarding αS's role in the SV fusion process. To better understand the reduction of rigidity within the membrane, or the reduction of gel phased lipid bilayers, a CF release assay was used to observe the impact of cholesterol on the liposome rearrangement within the bilayer [27]. As the liposome transitions from a fluid- to gel-like state, the internally quenched CF molecules escape upon rearrangement and ordering of the phospholipids. This rearrangement is related to an increase in percent efflux of CF, when passed through the bilayer transition temperature, due to protein binding and subsequent lipid rearrangement. Through use of the simplified synaptic mimic, POPE:SOPE:POPS, the rearrangement of lipids due to phospholipid head group interactions in the absence αS upon transitioning from fluid to gel states causes no change in CF efflux, seen in ***Figure 4.1 (left, black)***. This lack of CF efflux suggests an ideally mixed phospholipid bilayer, in which there are no interactions on the surface causing rearrangement of phospholipids. In the presence of αS there is a large increase in CF release from the liposome after passing through a fluid to gel transition, indicating that αS causes a rearrangement of phospholipids within the bilayer, allowing for CF escape during the fluid to get liposome transition (***Figure 4.1, left, green)***. This rearrangement of the phospholipids, or specific ordering of the membrane, is due to αS binding, but the extent to which this occurs in a true SV membrane remains unknown. The addition of the physiologically appropriate amount of cholesterol to the system shows a lack of CF release from the vesicle in the

absence and presence of αS, seen in ***Figure 4.1 (right, green)***. By adding cholesterol to a bilayer, the now liquid ordered phase causes a broadening in the observable transition, or less distinct, as cholesterol has the ability to induce ordering within the lipid bilayer. Cholesterol addition to the membrane is essential in understanding these complex mixtures, as 45% of the SV membrane is composed of cholesterol [40]. By adding an appropriate amount of cholesterol to the system, ordering of phospholipids is induced but is compensated by the presence of cholesterol, allowing for a more complex transition to the αS bound state. Cholesterol addition to the membrane induces the ordering transition by filling space between phospholipid tails, reaching a more rigid state of the bilayer, inhibiting CF release, as seen in ***Figure 4.1 (right)***. The dramatic change in CF release through the addition of cholesterol is significant to the sterols presence in physiological mixtures as a partner in keeping membrane rigidity upon reordering. Therefor, the lack of efflux seen in ***Figure 4.1 (right)*** is not indicative of lack of phospholipid rearrangement and order, but evidence that the ability for cholesterol to induce rigidity makes the αS-SV binding process more complex. The ability for cholesterol to create a less observable CF efflux transition of lipids makes αS's ability to inhibit the rigidity within the SV surface uncertain. When determining functional roles in the trafficking of vesicles, it is important to emphasize that αS's role in vesicle fusion is not solely dependent on the membrane rearrangement upon binding, as the addition of cholesterol causes stability within the bilayer when αS is bound.

The observed phospholipid-ordering of a liposome phase transition from the gel- to fluid-state of the bilayer was also observed through DSC to directly measure the energy of the bilayer transition (***Figure 4.2***). By continually transitioning a liposome of simplistic SV mimicked character through its gel to fluid-phase, a specific rearrangement and order of phospholipids occurs within the bilayer. This annealing of the membrane or specific equilibrated order is reached within the bilayer and allows for repeated observation through DSC (***Figure 4.2 black***). As was seen in the CF release assay experiments, a significant shift in the ordering of phospholipids

occurs upon binding of αS to the membrane (***Figure 4.1, left, green***) and upon binding of αS to the annealed liposome within the DSC cell, a shifted transition is apparent as phospholipids rearrange to a different ordering within the bilayer (***Figure 4.2, red***). The narrowing of the transition peak for both LUVs and SUVs in the presence of αS (***Figure 4.2, red***), indicates a shift to a more ordered bilayer from the wider, more mixed transition peak observed of liposomes in the absence of αS ***(Figure 4.2, black)***. The observed shifted transition is apparent as phospholipids rearrange to a more mixed or complex order within the bilayer [43].

Through direct integration of the DSC transition endotherm, the enthalpy (ΔH), transition temperature (Tm) and entropy (ΔS) of the liposome can be determined. The observed shift in energetics upon αS binding is directly represented as a shift in ΔH and Tm of the liposome. The observed shifted transition is apparent as phospholipids rearrange to a more mixed or complex order within the bilayer. Upon addition of a physiologically relevant amount of cholesterol to the liposomes, the transition from gel to fluid-states was not observable (not shown). The lack of an observable transition is consistent with CF release assay results (***Figure 4.1, right***), as cholesterol causes a smoother transition between states, weakening the sharpness of a transition and broadening the area. When high amounts of cholesterol are reached, the gel- to fluid- transition can become unobservable, and is indicated through CF and DSC results. The lack of observed transition does not indicate that it is absent, but indicates that it is again more complex. The energetic values represented in ***Table 4.3***, indicate a shift in enthalpy and melting temperature for both LUV and SUV mimicked liposomes. By also observing two sizes of liposomes, the significance of membrane curvature is also represented here, as ***Figure 4.2, left*** are LUVs, and ***Figure 4.2, right*** are SUVs. In comparison of curvature affect on the enthalpy and melting temperature change upon binding of αS, both transition shifts are consistent in narrowing upon binding, indicating a more ordered bilayer is obtained (***Figure 4.2, red***), but it is significant that when SUVs bind αS, there is a greater shift in enthalpy and melting temperature than when

bound LUVs (***Figure 4.2, left***). This greater shift indicates stronger interaction with SUV liposomes and more rearrangement influence due to high curvature, as the binding of αS to the surface is more responsive. Entropy is also represented in ***Table 4.3***, where a decrease in entropy or membrane disorder is seen when binding SUVs, again indicative of more order within the bilayer. A more ordered and shifted state was obtained through binding of αS, indicating the significance of curvature due to this peptides function.

4.5 Results and Discussion: conformational shifts in folded αS due to membrane complexity and curvature

It has been observed and further proposed that ordering of the phospholipids within the SV bilayer is effected upon binding of αS, but the conformation of the protein is also altered upon binding the membrane surface. αS holds a randomly coiled or intrinsically disordered structure in solution, and upon binding to the SV, α-helical structure is obtained. Small changes in phospholipid composition and vesicle diameter have vast effects upon the structural membrane bound conformer of αS. It has been previously observed that different levels of membrane bilayer curvature cause vast differences in the structure of αS [44]. CD spectroscopy was used to visualize the effect that curvature and complexity in liposomal mixture has on the structural properties of bound αS. 60:40 POPC:POPS LUVs, 60:40 POPC:POPS SUVs and SV mimicked SUVs were observed in the presence of αS through a temperature range of 37-91°C, ***Figure 4.3***. The peptide's bound α-helical character was observable for both POPC:POPS mixed liposome sizes (***Figure 4.3, A and B***), however, it is evident that SUV bound αS species depicts enhanced α-helical structure. By changing the size and curvature of the mimicked vesicle, αS reaches different bound conformers. When compared to the αS physiological environment, SUV sized SV mimicked liposomes were observed (***Figure 4.3, C***) but due to intensity of mixture complexity, light scattering of the signal caused an unobservable structure determination. However, the SUVs of the simple POPC:POPS mixture is relevant in comparison to a SV when indicating curvature significance. To more

clearly depict the strong curvature affects on conformer structure, LUV and SUV bound CD spectra are shown in ***Figure 4.4*** at 37°C, where SUV bound α-helical intensity is significant. A change in mimicked curvature to that of a physiological SV, is significantly important to obtain strong secondary structure formation of αS. Although lack of structure seen from the complex and accurate SV mimicked mixture (***Figure 4.3, C***), it is important to appreciate the dependence of the diameter size of the vesicles on structure formation (***Figure 4.3, A and B***) The curvature of an SUV sized vesicle, comparable to the appropriate diameter of a SV, is incredibly important in pulling out appropriate conformers of αS.

The sensitivity of αS to lipid rigidity (CF and transitional shifts) strongly suggests that the complex interplay of cholesterol-modulated lipid rigidity when combined with the equally dramatic impact of curvature (CD spectra) on rigidity within the context of the SV mimic will induce a distinct SV-induced αS conformation. A means to define how membrane properties modulate and induce distinct protein conformers, even when they are nearly or are intrinsically disordered is by observing the peptides folded to unfolded transition using DSC. Through the direct measure of the enthalpy of the ordered-to-disordered transition in the presence of membrane (the area under the curve in ***Figure 4.5***), a direct measure of the heat capacity change (ΔCp) as well as a direct measure of the Tm enables the probability to be calculated of the SV defined propensity of αS to be disordered or ordered, as induced by the SV membrane mimic.

In the presence of the SV membrane mimic, relevant in both complex lipid composition as well as SV curvature, that a robust endotherm is observed (***Figure 4.5***). By contrasting this robust signal to that of the equivalent experiment with a simple binary lipid mixture comprised of POPC:POPS, there was a complete absence of an αS endotherm. This is extremely significant as CD carried out in the presence of POPC:POPS clearly shows α-helical content. As high cholesterol content of the SV membrane mimic scatters the CD signal (***Figure 4.3, C***) and

obfuscates the αS signal, the ability to then measure this complex mixture's effect on conformer formation via DSC is significant to this study.

Through use of the Gibbs-Helmholtz equation that was constrained by the experimentally defined DSC enthalpy, heat capacity change and transition temperature, the free energy (ΔG) at physiological temperature associated with αS induced by the SV membrane mimic was calculated (***Table 4.4***). It is the energetic of free energy that reveals the propensity of αS to sample disordered states when associated with the SV membrane mimic where fraction folded = 1/1+e(- ΔG/RT). ***Figure 4.6*** displays the free energy profile of the bound state to a physiologically relevant SV mimic, more clearly representing the probability of αS to sample disordered states when bound to the SV membrane mimic. At physiological temperature and when bound to the SV membrane mimic with high curvature, a significant fraction (~10%) of αS is disordered. Such disordered protein states are implicated in formation of tangled aggregates (toxic oligomers) at the membrane surface.

4.6 Closing comments

The role of lipid rigidity with regard to lipid phase behavior, organization and curvature in the presence and absence of αS is observable through the CF release assay, DSC and CD studies. It is apparent that the αS binding process and role in trafficking of SVs is incredibly complex, causing significant changes within the bilayer order upon binding. This bilayer ordering is significant in the measurement of membrane rigidity in that the ordering of phospholipids and cholesterol would cause changes in membrane behavior. The difference in conformers of αS formed upon binding, are dependent both on membrane mixture and liposome curvature. The role of the SV membrane mimic on αS conformers is apparent and significant, in that small changes in liposome complexity and diameter produce vast changes in conformational characteristics. The changes in αS conformer formation might play a role in binding affinity and functional properties related to the rigidity of the vesicle.

Rigidity of lipid bilayers is subject to fluctuation due to direct observation of lipid ordering and strong differences in αS conformer formation induced by different phospholipid mixtures and curvature. Further experiments are necessary using physiologically relevant phospholipid mixtures and liposome sizes to directly measure the αS conformer's affect on SV rigidity. However it is important to emphasize the significance of the drastic changes within membrane order and observed αS conformer formation due to binding, a direct effect to its function in the SV fusion process.

Illustrations:

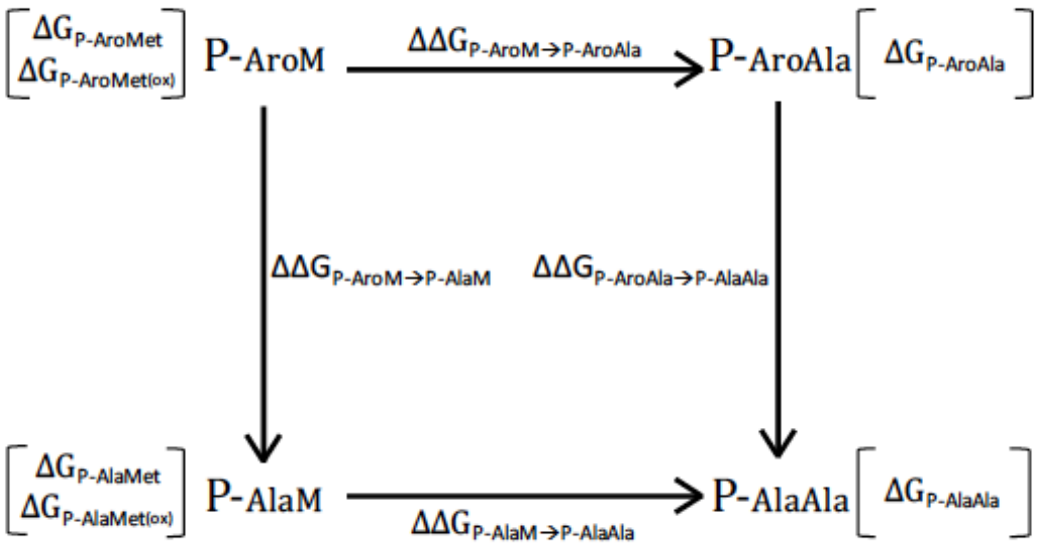

Figure 2.1: Thermodynamic double mutant cycle example of Aromatic-Methionine (AroMet) peptides. Nomenclature is: Wild-type peptide (AroMet and AroMet(ox)), singly mutated peptide (AlaMet and AlaMet (ox)) and doubly mutated peptide (AlaAla). Aro, Met/M and Ala represent aromatic residue, methionine (un-oxidized or oxidized) and alanine, respectively. Free energy of each peptide denaturation is represented as ΔG at each step in the cycle. ΔΔG values are determined by the difference in ΔG denaturation values of peptides at 0°C, which were used to determine the $\Delta\Delta\Delta G_{Int}$.

Table 2.1: All peptides used in CD thermal studies, their appropriate abbreviation and their construct sequence of only 15 residues varying only at residue 9 and 13 of the aromatic and Met residue represented in **bold**.

Peptide	***Abbreviation***	***Construct Sequence***
Tyr-Met	YM	YGGSAAEA-**Y**-AKA-**M**-AR-NH_2
Tyr-Met (ox)	YM (ox)	YGGSAAEA-**Y**-AKA-**M (ox)**-AR-NH_2
Phe-Met	FM	YGGSAAEA-**F**-AKA-**M**-AR-NH_2
Phe-Met (ox)	FM (ox)	YGGSAAEA-**F**-AKA-**M (ox)**-AR-NH_2
Tyr-Ala	YA	YGGSAAEA-**Y**-AKA-**A**-AR-NH_2
Phe-Ala	FA	YGGSAAEA-**F**-AKA-**A**-AR-NH_2
Ala-Met	AM	YGGSAAEA-**A**-AKA-**M**-AR-NH_2
Ala-Met (ox)	AM (ox)	YGGSAAEA-**A**-AKA-**M (ox)**-AR-NH_2
Ala-Ala	AA	YGGSAAEA-**A**-AKA-**A**-AR-NH_2

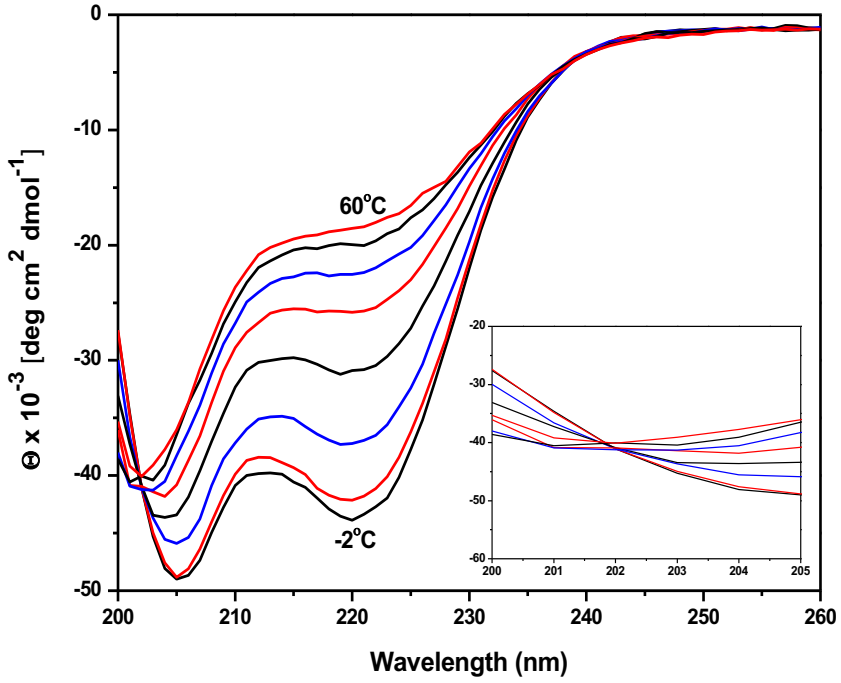

Figure 2.2: Combined spectra of one peptide observed from 200 to 260nm at increasing temperatures from -2°C to 60°C. Crossing of all spectra at ~202nm indicates isodichroic point more clearly indicated in inset plot.

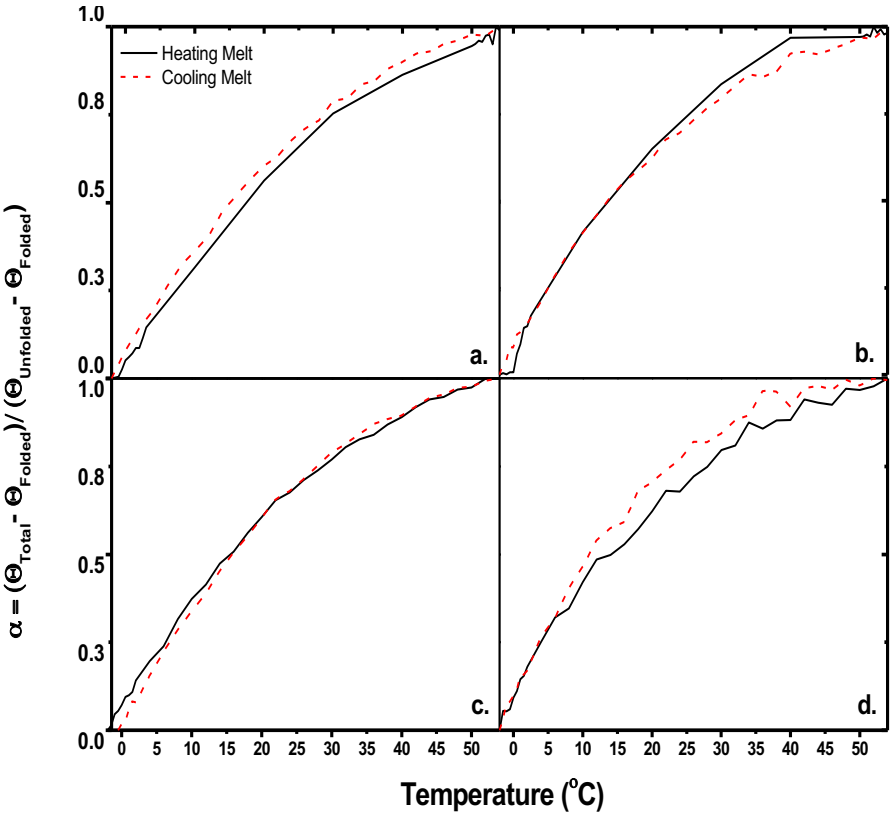

Figure 2.3: Overlaid heating and cooling melt curves for YM, YM (ox), FM, and FM (ox) peptides. Heating curves represented by **black solid line**, and cooling curves represented by **red dashed line**. Ellipticity displayed as a fraction of unfolded peptide (α, equation 2.3): **a.** YM heating and cooling melt, **b.** YM (ox) heating and cooling melt, **c.** FM heating and cooling melt, **d.** FM (ox) heating and cooling melt.

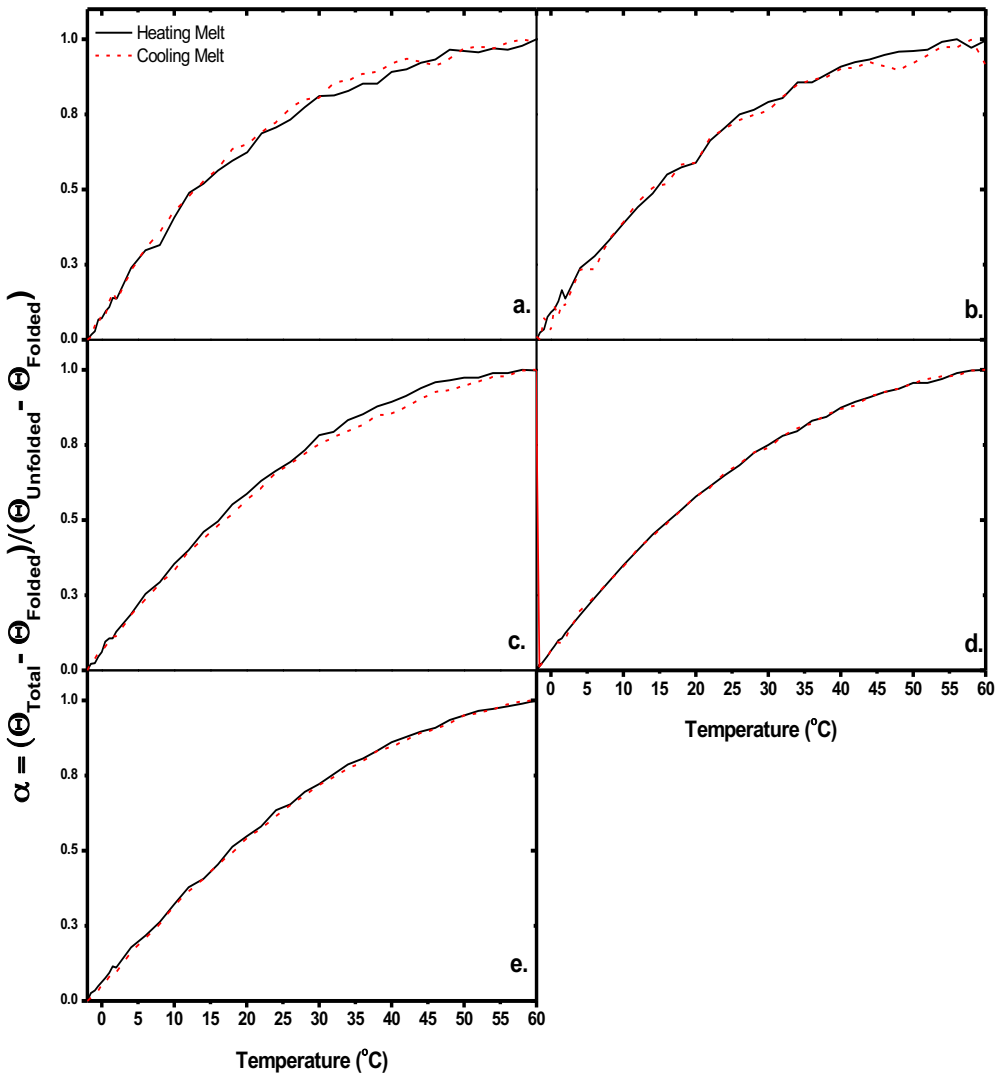

Figure 2.4: Overlaid heating and cooling curves for YA, FA, AM, AM (ox), and AA peptides. Heating curves represented by **black solid line**, and cooling curves represented by **red dashed line**. Ellipticity displayed as a fraction of unfolded peptide (α, equation 2.3): **a.** YA heating and cooling melt, **b.** FA heating and cooling melt, **c.** AM heating and cooling melt, **d.** AM (ox) heating and cooling melt, **e.** AA heating and cooling melt.

Table 2.2: Thermodynamic parameters obtained for the YM and YM (ox) peptides. $\Delta H_{Tm,\ CD}$ is the enthalpy obtained from fitting the CD denaturation data and $\Delta H_{Tm,\ DSC}$ is the enthalpy measured through DSC.

	$\Delta H_{Tm,\ CD}$ (kcal/mol)	**Tm (°C)**	**ΔCp (kcal/mol°C)**	**$\Delta H_{Tm,\ DSC}$ (kcal/mol)**	**Tm (°C)**	**ΔCp (kcal/mol°C)**
Tyr-Met	17.54 ± 0.01	15.8 ± 0.2	0.17 ± 0.01	16.6	20.5	0.186
Tyr-Met (ox)	20.9 ± 0.2	13.4 ± 0.6	0.19 ± 0.02	19.7	14.9	0.183

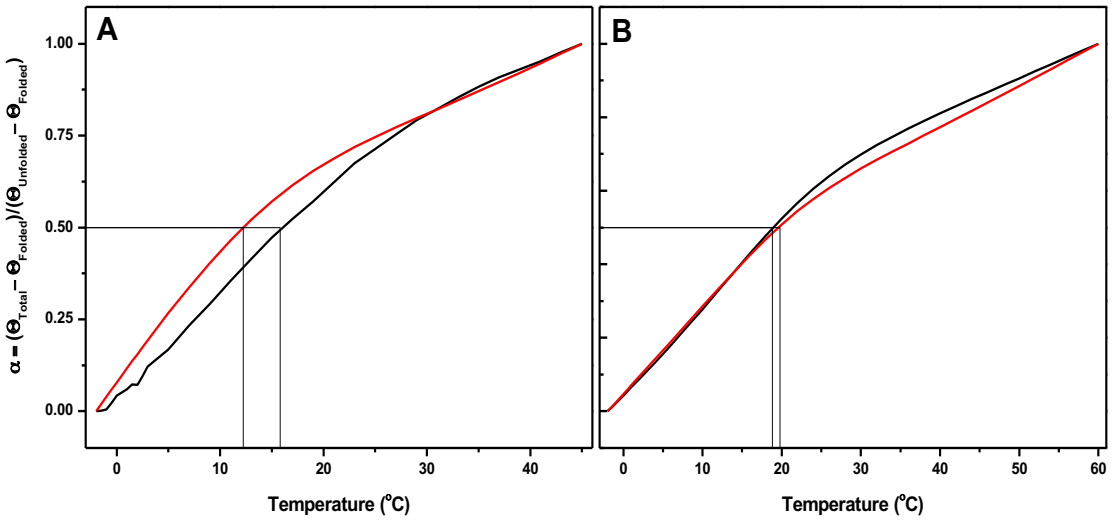

Figure 2.5: CD thermal denaturation fit curves for: **a.** YM as **black solid line** and YM (ox) as **red solid line**, **b.** FM as **black solid line** and FM (ox) as **red solid line**. The **black lines** at α = 0.5 (equation 2.3) display the melting temperature of all four peptides in both plots **a** and **b**.

Table 2.3: Determined $\Delta H_{Tm,\ CD}$ (kcal/mol), ΔCp (kcal/molK) and Tm (°C) of each YM, YM (ox), FM and FM (ox) through thermodynamic analysis of CD thermal denaturation curves.

	Tyr-Met	**Tyr-Met (ox)**	**Phe-Met**	**Phe-Met (ox)**
$\Delta H_{Tm,\ CD}$ (kcal/mol)	17.54 ± 0.01	20.9 ± 0.2	26.0 ± 0.7	27.1 ± 0.1
ΔCp (kcal/mol°C)	0.17 ± 0.01	0.19 ± 0.02	0.2 ± 0.2	0.21 ± 0.02
Tm (°C)	15.8 ± 0.2	13.4 ± 0.6	18.3 ± 0.3	21 ± 1

Table 2.4: Determined $\Delta H_{Tm,\ CD}$ (kcal/mol), ΔCp (kcal/molK) and Tm (°C) of each YA, FA, AM, AM (ox), AA through thermodynamic analysis of CD thermal denaturation curves.

	Tyr-Ala	**Phe-Ala**	**Ala-Met**	**Ala-Met (ox)**	**Ala-Ala**
$\Delta H_{Tm,\ CD}$ (kcal/mol)	11.94 ± 0.01	11.92 ± 0.01	24.35 ± 0.00	18.69 ± 0.03	17.20 ± 0.03
ΔCp (kcal/mol°C)	0.12 ± 0.00	0.15 ± 0.00	0.06 ± 0.02	0.17 ± 0.02	0.24 ± 0.01
Tm (°C)	12.3 ± 0.8	12.4 ± 0.7	18.0 ± 0.9	18.7 ± 0.8	21.4 ± 0.9

Table 2.5: Determined $\Delta\Delta\Delta G_{Int}$ for YM, YM (ox), FM and FM (ox) at 0°C where the peptide is in the fully ordered or fully folded α-helical state.

Peptide	***$\Delta\Delta\Delta G_{int}$ (kcal/mol)***
Tyr-Met	-0.01
Tyr-Met (ox)	0.41
Phe-Met	0.62
Phe-Met (ox)	1.24

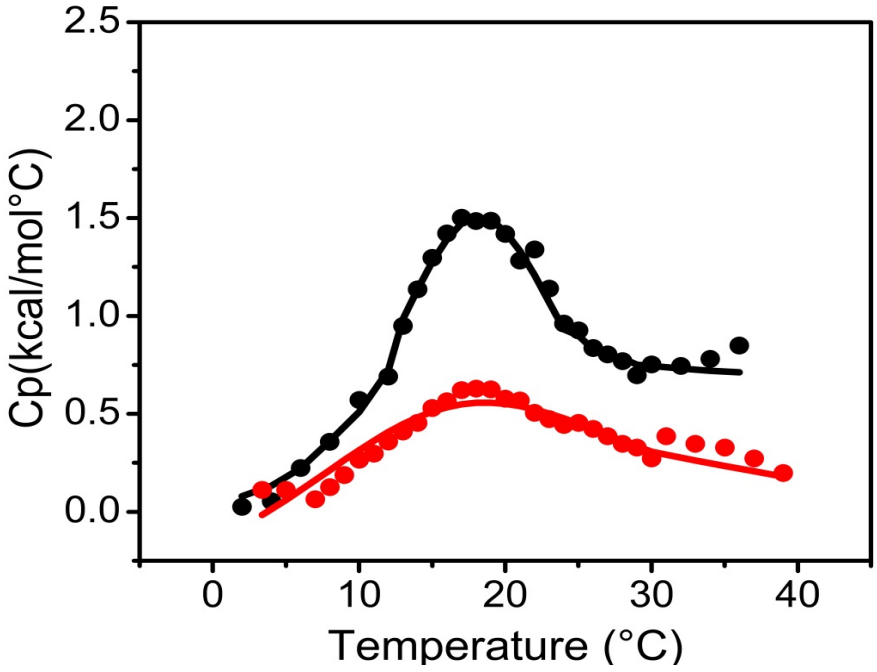

Figure 2.6: Raw DSC data obtained for 100μM of the un-oxidized peptide construct (**red dots**), and 150μM of the oxidized peptide construct (**black dots**) in a buffer composed of 10mM KH_2PO_4 and 100mM KCl at a pH of 7.5 The **solid red** and **black** lines represent the fits for the un-oxidized and oxidized construct respectively. This data was used to constrain the fit values of the CD.

Table 3.1: Stability parameters obtained for C2 domains of Syt I and both isoforms of the C2A domain in Dys. The top portion of the table includes human Syt I and Dys data summarized from previous denaturation studies [18, 19, 20], as well as new measurements for cotton Syt I C2A. The parameters reported for the human Syt I C2A domain, in the top half of the table, were collected with the construct containing the amino acids 140-265. The lower portion of the table shows the stability parameters for the human Syt I C2A construct containing residues 96-265, in the presence of phospholipid bilayers of different compositions and size. All ΔG values reported represent free energy of stability at 37°C.

Previously Studied C2 Domains in Absence of Ligand					
	ΔH(kcal/mol)	ΔCp(kcal/mol·K)	T_m(°C)	$\Delta G_{37°C}$ (kcal/mol)	ΔS(kcal/mol·K)
Syt I C2A	58.7±0.3	1.92±0.09	55.99±0.04	2.32±0.05	0.178±0.006
Syt I C2B	69.6±0.6	2.19±0.04	46.4±0.1	1.74±0.09	0.22±0.01
Cotton Syt I C2A	2.5±0.1	0.37±0.09	39.5±0.1	0.017±0.01	0.008±0.004
Dys C2A	12.6±0.8	0.97±0.01	42.2±0.6	0.17±0.02	0.040±0.002
Dys C2Av1	18.3±0.4	1.32±0.01	55.6±0.1	0.33±0.02	0.058±0.001
Human Syt I C2A (96-265) in Presence of Lipid					
	ΔH(kcal/mol)	ΔCp(kcal/mol·K)	T_m(°C)	$\Delta G_{37°C}$(kcal/mol)	ΔS(kcal/mol·K)
POPC:POPS(60:40)	59.2±0.2	1.91±0.04	53.32±0.03	2.18±0.02	0.181±0.004
POPC:POPS(60:40) and Ca^{2+}	58.6±0.4	4.50±0.03	68.96±0.06	-1.50±0.01	0.171±0.007
(POPC:POPS):cholesterol (80:20):30	67.9±0.2	3.08±0.02	68.04±0.04	1.67±0.01	0.199±0.003
Membrane Domain LUV and Ca^{2+}	135.7±0.5	3.58±0.01	68.6±0.6	7.09±0.06	0.413±0.02
Membrane Domain SUV and Ca^{2+}	140.8±0.6	3.60±0.02	75.3±0.6	7.60±0.02	0.429±0.01
Synaptic Mimic and Ca^{2+}	107.0±0.1	2.75±0.06	67.36±0.01	5.75±0.02	0.315±0.001

Table 3.2: Phospholipid components in the membrane domain forming mixture (left columns), as well as the phospholipid components of the SV mimic mixture, where FA1 and FA2 represent the acyl chains attached to the glycerol backbone. These lipid compositions are based off of those presented in [33], and are designed to capture the essence of the lipid diversity of the SV outer leaflet. The percentages listed for each phospholipid species represent the mole percent of that species within the total phospholipid mixture, while the percent given for cholesterol represents the mole percent found within the total mixture.

Membrane Domain Forming Mixture				**Synaptic Vesicle Mimic Mixture**			
PE ratio	*FA1*	*FA2*	*% Total Phospholipid*	*PE ratio*	*FA1*	*FA2*	*% Total Phospholipid*
3	16;0	18;1	38	3	16;0	18;1	38
2	18;0	18;1	25	2	18;0	18;1	25
1	18;0	22n6	13	1	18;0	22n6	13
PI ratio	*FA 1*	*FA2*	*% Total Phospholipid*	*PI ratio*	*FA 1*	*FA2*	*% Total Phospholipid*
2	18;0	18;0	1	-	-	-	-
1	18;1	18;1	0.5	1	18;1	18;1	0.5
2	16;0	18;1	1	2	16;0	18;1	1
1	18;0	20;4	0.5	1	18;0	20;4	0.5
PS ratio	*FA 1*	*FA2*	*% Total Phospholipid*	*PS ratio*	*FA 1*	*FA2*	*% Total Phospholipid*
3	16;0	16;0	7	-	-	-	-
1	18;0	22n6	2	1	18;0	22n6	12
2	18;0	18;1	5	2	18;0	18;1	10
3	16;0	18;1	7	-	-	-	-
Cholesterol	-	-	45%	Cholesterol	-	-	45%

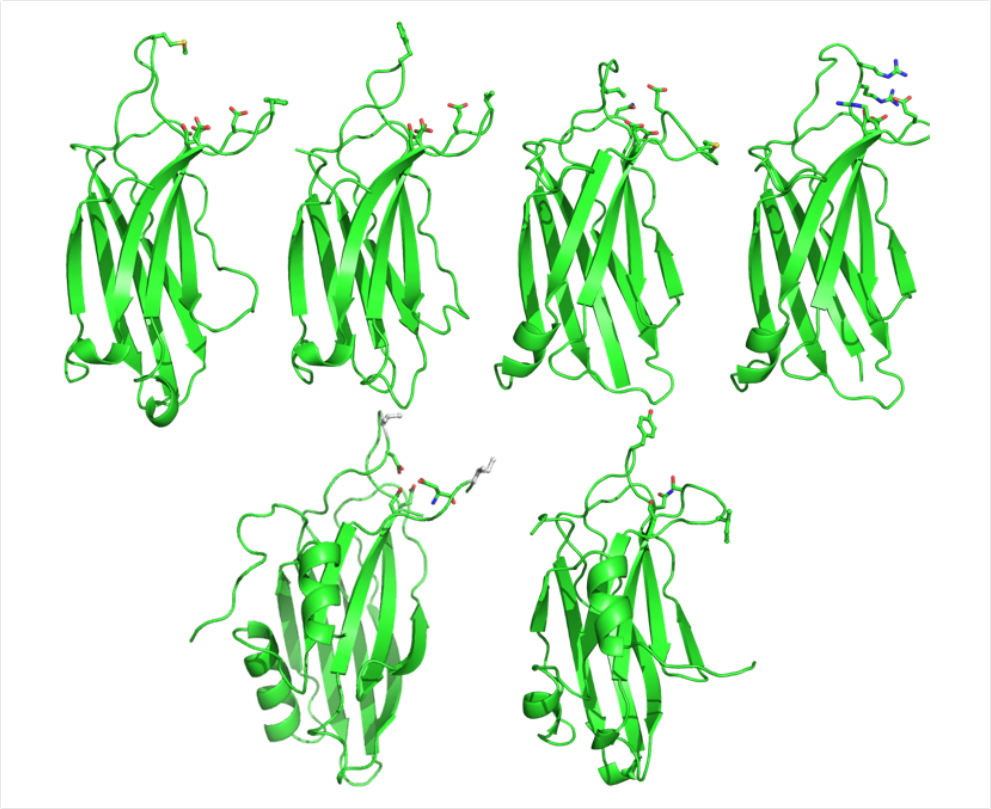

Figure 3.1: Structures of various C2 domains. The top row of structures correspond to C2A domains (from left to right) of human Syt I, cotton Syt I, human canonical Dys, and human variant Dys. The bottom row of structures are C2B domains (from left to right) from human and cotton Syt I. The calcium binding residues are shown and the putative lipid interacting residues are in white balls-and-sticks. Note the high level of structural similarity.

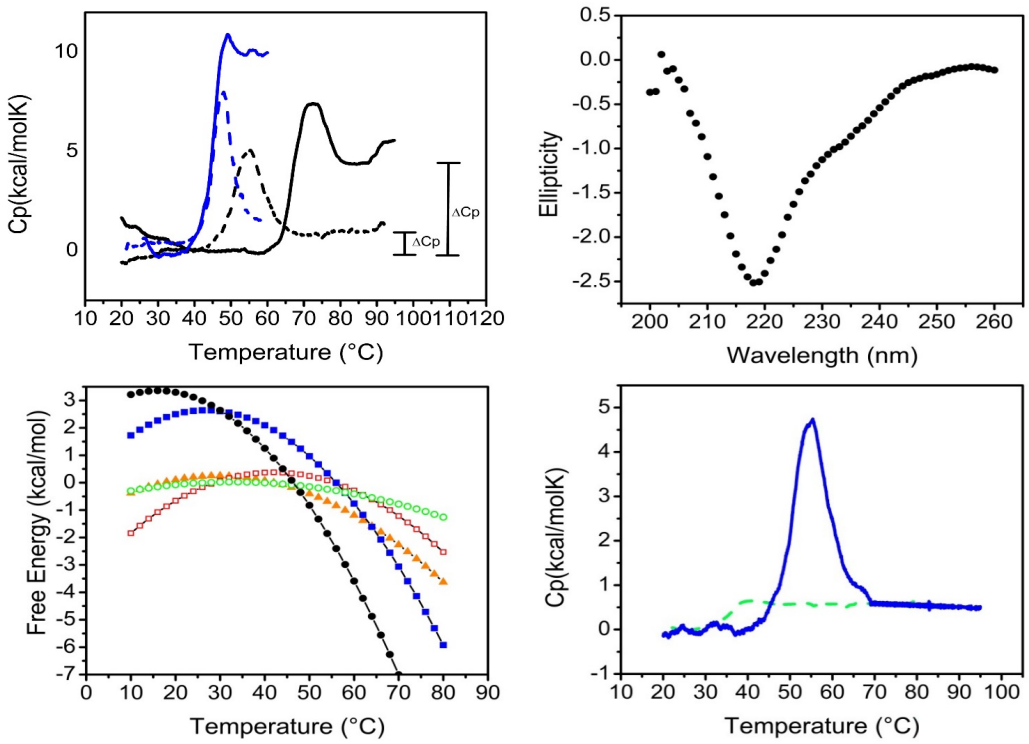

Figure 3.2: ***Upper Panels:*** The left panel shows the denaturation profile of human Syt. I C2A (residues 96-265) at 13µM in the presence of 1mM LUVs composed of POPC:POPS (60:40) and with either 1mM EGTA (**dashed black line**) or 1mM Ca2+ (**solid black line**). Also shown is 11µM C2B in the presence of 490µM LUVs composed of (95:5) POPC:PIP2 (**solid blue line**), 13µM C2B in the presence of 0.5 mM EGTA (**dashed blue line**). The large ΔCp differences are highlighted for the C2A domain with brackets (left panel). The right panel is the CD spectrum obtained for the C2A domain (residues 96-265) in the presence of 700 μM LUVs composed of POPC:POPS (60:40) and 1mM Ca2+. ***Lower Panels:*** The left panel shows the free energies stabilities of several C2 domains, in the absence of ligand, over a range of temperatures. These stabilities were calculated through the use of the Gibbs-Helmholtz equation, utilizing the ΔH, ΔCp, and Tm obtained from the thermal denaturation profiles of the domains. The **orange triangles**, **red squares**, **blue squares**, **green circles** and **black circles** represent canonical C2A Dys, C2Av1 Dys, human Syt I C2A (residues140-265), cotton Syt I C2A, and human Syt I C2B, respectively. The right panel shows the denaturation profile of the cotton C2A domain [Cotton C2A] = 175µM) with that of the human Syt I C2A domain construct containing the amino acids 140-265 (blue; [Human C2A] = 13µM) in the presence of 1mM EGTA. The **blue** and **green** lines under the curves represent the baselines used for integration.

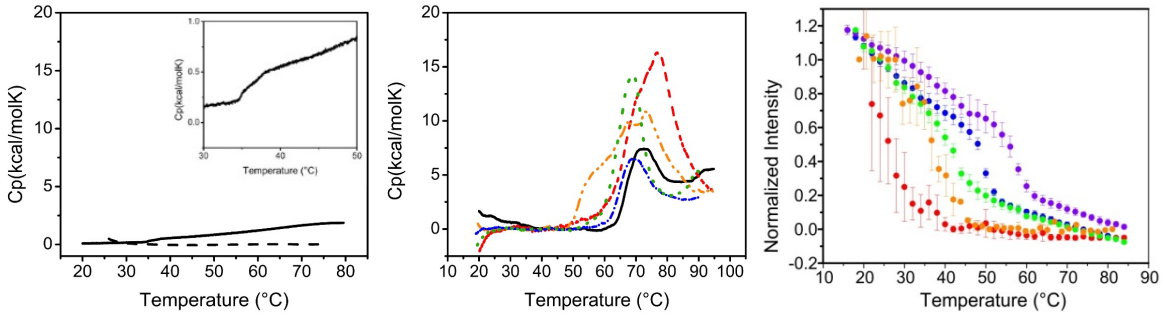

Figure 3.4: ***Left Panel*****:** Thermograms obtained for LUVs of the membrane domain forming lipid mixture, at a phospholipid concentration of 3.3mM (**solid black line**) and the SV mimic mixture at a phospholipid concentration of 1mM (**dashed black line**). The inset in the upper right is a close-up of the phase transition. ***Middle Panel*****:** Denaturation profiles of 13 µM human Syt I C2A (residues 96-265) in the presence of 1 mM LUVs (unless stated otherwise) of different lipid compositions and 1mM Ca^{2+}. **solid black line** represents the denaturation with POPC:POPS (60:40); **blue dashed and dotted line** represents the denaturation with (POPC:POPS):cholesterol (80:20):30; **yellow dashed and dotted line** represents denaturation with the membrane domain forming lipid mixture from ***Table 3.1***; the **red dashed line** represents the denaturation with the membrane domain forming lipid mixture as SUVs; and **green dotted line** represents the denaturation with the SV mimic from ***Table 4.1***. All DSC scans were conducted in a buffer composed of 20mM MOPS and 100mM KCl at a pH of 7.5. ***Right Panel*****:** FLT denaturation of C2AB fragment of Syt I in the presence of membrane with or without Ca^{2+}. **Red:** 0.75μM C2AB, 5.1mM Ca^{2+}, 110μM LUVs (60:40, POPC:POPS). **Orange:** 0.9μM C2AB, 600μM Ca^{2+}, 1.2mM LUVs (60:40, POPC:POPS). **Green:** 0.75μM C2AB, 110μM LUVs (60:40, POPC:POPS), 500μM EGTA. **Blue:** 0.75μM C2AB, 210μM LUVs (95:5, POPC:PIP2), 500μM EGTA. **Purple:** 0.75μM C2AB, 5.1mM Ca^{2+}, 210μM LUVs (95:5, POPC:PIP2). Right panel adapted from [18].

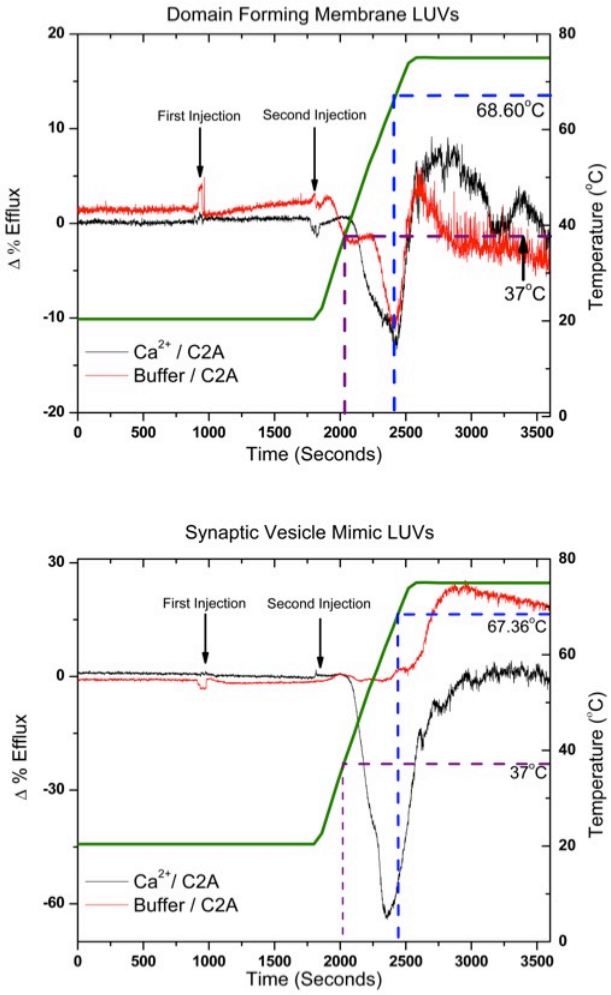

Figure 3.4: Change in the percent efflux of carboxyfluorescein from 200μM LUVs composed of a SV mimic lipid mixture (bottom) and LUVs composed of domain forming lipid mixture (top) injected with Ca^{2+} at 15 min and human Syt C2A domain (residues 96-265) at 30 min to final concentrations of 3mM and 13.33μM respectively. Δ%Efflux was calculated by subtracting control titrations in which no protein was added during the second injection. Arrows indicate the addition of Ca^{2+} (1^{st} injection), or protein (2^{nd} injection) during the course of equilibration. For titration controls in which Ca^{2+} or protein were not present the injections were made with buffer composed of 20mM MOPS, 100mM KCl, 0.02% NaN_3, pH of 7.5. For all titrations the temperature was held constant at 20.4C until equilibration of the second injection when it was set to increase to 75˚C. The green line represents the temperature change over time, while the blue and purple dashed lines represent the temperatures (and corresponding titration times) at which the membrane phase transition occurs (purple) and the bound-protein denatures (blue). The efflux conditions for both plots were as follows: the **black solid line** represents the Δ%efflux in the presence of both the human Syt I C2A (residues 96-265) and Ca^{2+}, and the **red solid line** represents the Δ%efflux of the domain in the absence of Ca^{2+}.

Table 4.1: Physiological mimicked mixture of SVs, comprised of PE, PI, PS and cholesterol. Percent total phospholipid comprised of PE, PI and PS, where percent cholesterol is a mole percentage of total phospholipid (55% total phospholipid, 45% cholesterol).

Synaptic vesicle mimic mixture			
	FA1	**FA2**	**% Total Phospholipid**
PE Ratio			
3	16:00	18:01	38
2	18:00	18:01	25
1	18:00	22:06	13
PI Ratio			
1	18:01	18:01	0.5
2	16:00	18:01	1
1	18:00	20:04	0.5
PS Ratio			
1	18:00	22:06	12
2	18:00	18:01	10
Cholesterol	**-**	**-**	**45**

Table 4.2: Simplified SV mixture, comprised of PE, PS and cholesterol. Percent total phospholipid comprised of PE and PS, where percent cholesterol is a mole percentage of total phospholipid (55% total phospholipid, 45% cholesterol).

Simplified synaptic vesicle mimic mixture			
	FA1	**FA2**	**% Total Phospholipid**
POPE	16:00	18:01	38
SOPE	18:00	18:01	38
POPS	16:00	18:01	24
Cholesterol	-	-	45

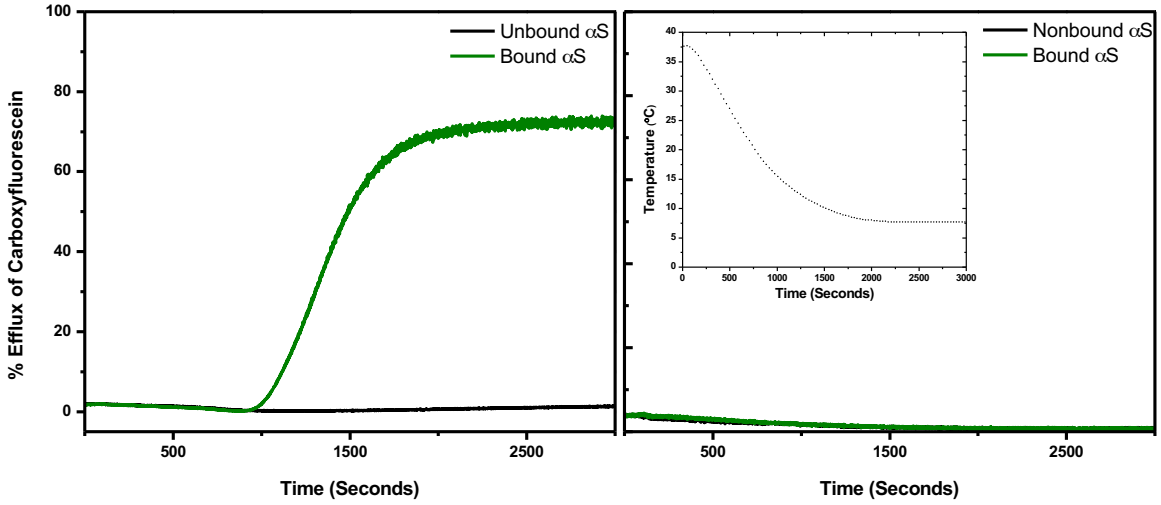

Figure 4.1: CF release assay of 200μM CF containing liposomes at 200nm LUV diameter. αS containing samples contain 0.8μM peptide and 200μM CF containing liposomes. Unbound αS and bound αS containing samples were run from 40°C to 0°C through the phospholipid bilayer transition temperature calculated to be approximately 27°C. 38:38:24 POPE:SOPE:POPS liposomes in the presence (**green**) and absence (**black**) of αS (**left panel**); and (38:38:24):45 (POPE:SOPE:POPS):Cholesterol in the presence (**green**) and absence (**black**) of αS (**right panel**). Time to temperature conversion is plotted and inset on **right panel**.

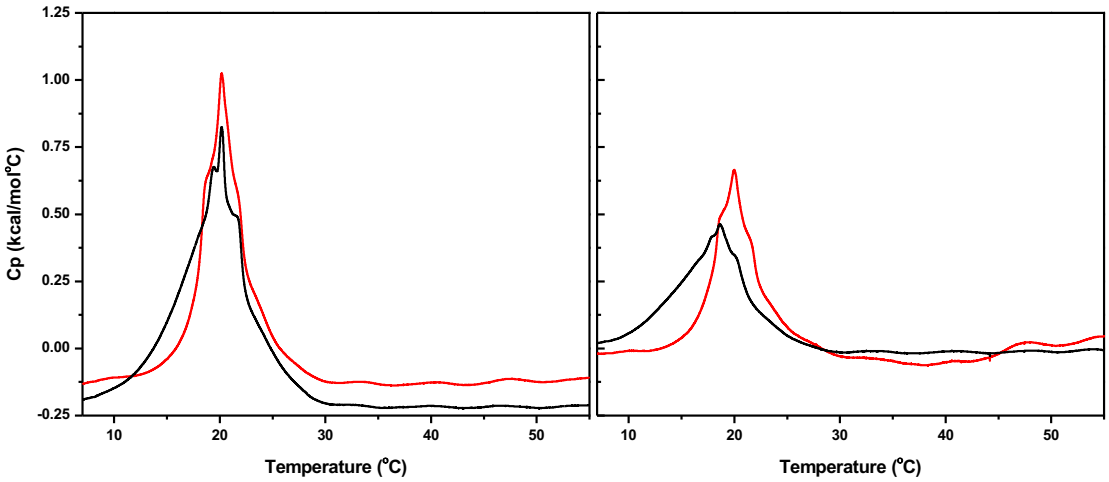

Figure 4.2: Heating thermograms of 38:38:24 POPE:SOPE:POPS LUVs (left) and SUVs (right) in the presence (**red**) and absence (**black**) of bound αS. All scans were conducted at a phospholipid concentration of 10mM, in 20mM MOPS, 100mM KCl, pH 7.5 buffer. Upon addition of αS to the LUV mixture, corrections in molar phospholipid concentration were accounted for. Scans are normalized to the appropriate phospholipid concentration in each case.

Table 4.3: Calculated enthalpy (ΔH), melting temperature (Tm) and entropy (ΔS) values for 38:38:24 POPE:SOPE:POPS LUV-bound and unbound αS, 38:38:24 POPE:SOPE:POPS SUV-bound and unbound αS endotherms in Figure 4.2.

Lipid Mixture	**ΔH (kcal/mol)**	**Tm (°C)**	**ΔS (kcal/molK)**
38:38:24 POPE:SOPE:POPS LUV *Unbound αS*	3.43	19.6	0.0117
38:38:24 POPE:SOPE:POPS LUV *Bound αS*	3.63	20.3	0.0124
38:38:24 POPE:SOPE:POPS SUV *Unbound αS*	3.43	17.8	0.0118
38:38:24 POPE:SOPE:POPS SUV *Bound αS*	3.00	20.1	0.0102

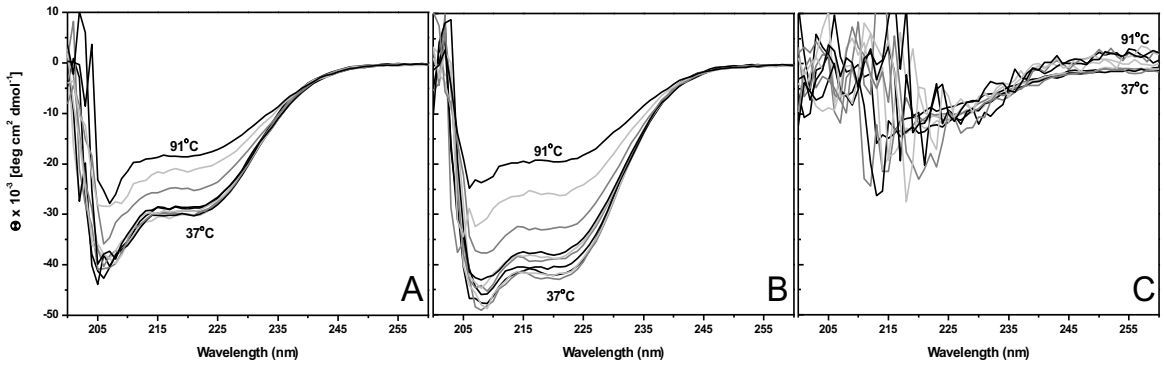

Figure 4.3: CD spectra from thermal denaturation of αS in the presence of different liposome mixtures and curvature sizes. Thermal denaturation observed from 37°C to 91°C. A) 15μM αS in the presence of LUVs (60:40 POPC:POPS) at a 250:1 [L]:[P] ratio, where strongest α-helical structure observed at 37°C; B) 15μM αS in the presence of SUVs (60:40 POPC:POPS) at a 375:1 [L]:[P] ratio, where strongest α-helical structure observed at 37°C; C) 5μM αS in the presence of synaptic vesicle mimicked SUVs at a 200:1 [L]:[P] ratio, where secondary structure determination is unclear.

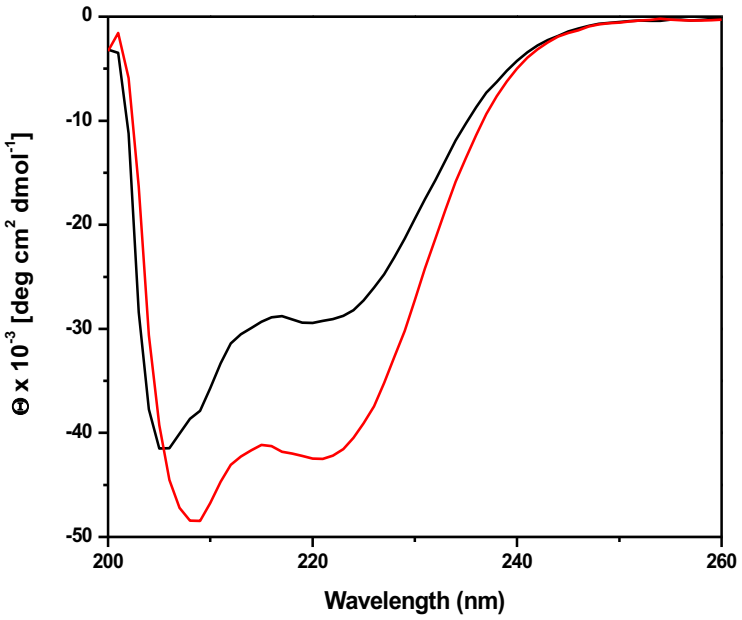

Figure 4.4: Average of three CD spectra at 37°C, 39°C and 41°C where the strongest helical content was observed, of 15μM αS in the presence of LUVs (**black**) at a 250:1 [L]:[P] ratio, and SUVs (**red**) at a 375:1 [L]:[P] ratio. LUVs and SUVs were of a 60:40 POPC:POPS phospholipid mixture.

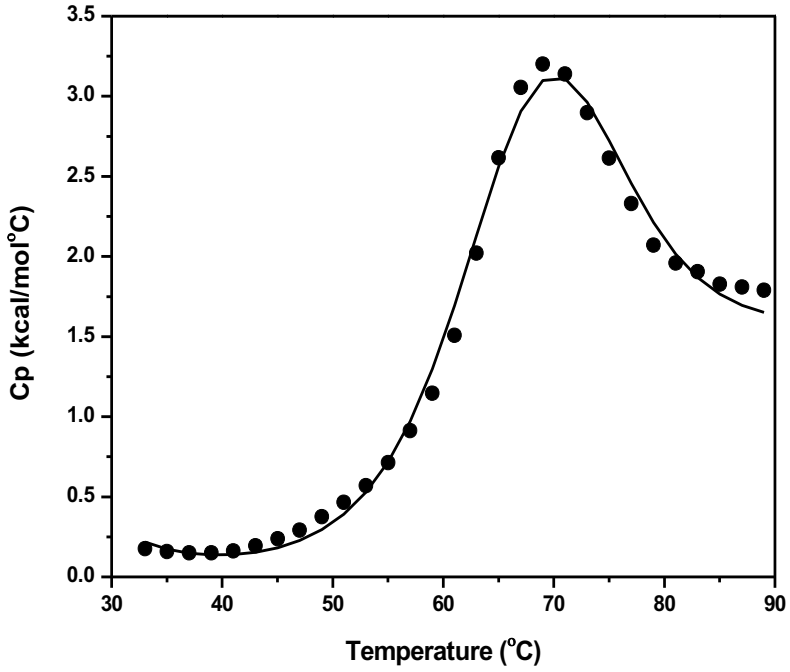

Figure 4.5: Heating thermogram of 20μM αS in the presence of synaptic vesicle mimicked SUVs at a 200:1 [L]:[P] ratio from 35-90°C. Raw data represented as **black circles**, and model fit line represented as **black solid line**.

Table 4.4: Calculated enthalpy (ΔH), heat capacity change (ΔCp), melting temperature (Tm) and free energy at body temperature ($\Delta G_{37°C}$) values for 20μM αS in the presence of SV mimicked SUVs at a 200:1 [L]:[P] ratio, from Figure 4.6 heating thermogram.

ΔH	40.1 kcal/mol
ΔCp	1.5 kcal/mol°C
Tm	65.04 °C
$\Delta G_{37°C}$	1.4 kcal/mol

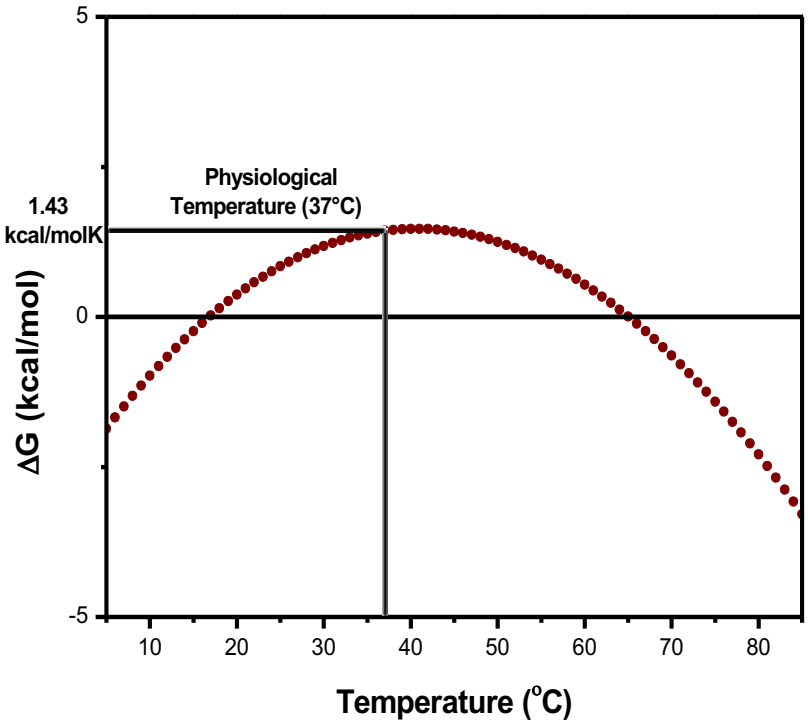

Figure 4.6: Free energy stability plot of αS in the presence of SV mimicked SUVs. Stabilities were calculated using the Gibbs-Helmholtz equation, utilizing ΔH, ΔCp and Tm obtained from the DSC thermal denaturation profile.

Thesis Conclusions:

Through peptide and membrane binding studies, various situations have been observed indicating the strong influence of internal sequence changes and membrane binding, to the secondary structure of proteins. Through a DMC analysis, the hypothesis of increased structural stability within a protein's folded structure due to the oxidation of Met in an aromatic-Met interaction is consistent with observed experimental results, and the increase in structural stability is strictly due to these two side chain interactions. The DMC was a means to clarify that the aromatic-Met interaction was the sole contributor to the increase in structural strength. Through membrane binding studies of various domains of Syt I, a stronger understanding of membrane-protein interplay was observed and more clearly defined. Different conformers of Syt I domain were observed through the use of varying lipid mixtures, as well as direct informational content changes within the bilayer. This observation of membrane composition affecting obtained folded protein conformers was consistent also with αS results. It is evident that the binding of αS to various lipid mixtures and curvature strengths induces significant changes in the resulting folded conformer of αS. These different conformers also have an interplay affect within the membrane to cause reordering of phospholipids within the bilayer, suggesting more complex interaction that is consistent with the hypothesis of decreased SV rigidity. Although rigidity was not directly observed, these studies can be used to direct future experiments that test the rigidity of the bilayer upon αS binding.

References:

[1] Valley, C.C. et al (2012). The Methionine-aromatic Motif Plays a Unique Role in Stabilizing Protein Structure, *J Biol Chem* **287**, 34979-91.

[2] Reid, K.S.C., Lindley, P.F. & Thornton, J.M. (1985). Sulphur-aromatic interactions in proteins. *FEBS Letters* **190**, 209-213.

[3] Viguera, A.R. & Serrano, L. (1995). Side-chain interactions between sulfur-containing amino acids and phenylalanine in α-helices. *Biochemistry* **34**, 8771-8779.

[4] Van Deventer, S.J. (1997) Tumour necrosis factor and Crohn's disease. *Gut* **40**, 443-8.

[5] Liebregts, T. et al (2007). Immune activation in patients with irritable bowel syndrome. *Gastroenterology* **132**, 913-20.

[6] Cantin, A.M., North, S.L., Fells, G.A., Hubbard, R.C. & Crystal, R.G. Oxidant-mediated epithelial cell injury in idiopathic pulmonary fibrosis. *J Clin Invest* **79**, 1665-73 (1987).

[7] Maier, K., Leuschel, L. & Costabel, U. Increased levels of oxidized methionine residues in bronchoalveolar lavage fluid proteins from patients with idiopathic pulmonary fibrosis. *Am Rev Respir Dis* **143**, 271-4 (1991).

[8] Wong, P.S. & Travis, J. Isolation and properties of oxidized alpha-1-proteinase inhibitor from human rheumatoid synovial fluid. *Biochem Biophys Res Commun* **96**, 1449-54 (1980).

[9] Szatrowski, T.P. & Nathan, C.F. Production of large amounts of hydrogen peroxide by human tumor cells. *Cancer Res* **51**, 794-8 (1991).

[10] Palmer, H.J. & Paulson, K.E. Reactive oxygen species and antioxidants in signal transduction and gene expression. *Nutr Rev* **55**, 353-61 (1997).

[11] Horovitz, A., Serrano, L., Avron, B., Bycroft, M., Fersht, A. (1990) Strength and cooperativity of contributions of surface salt bridges to protein stability, *J. Mol. Biol.* 216, 1031-1044.

[12] Serrano, L., Bycroft, A., Fersht, A. (1991). Aromatic-aromatic interactions and protein stability investigation by double-mutant cycles. J. Mol. Biol. 218, 465-475.

[13] Horovitz, A. Double mutant cycles: a powerful tool for analyzing protein structure and function, *Folding and Design*, 1, 121-126

[14] Correa, D. H. A.; Ramos, C. H. I. The use of circular dichorism spectroscopy to study protein folding, form and function. *Afr. J. Biochem. Res.* 2009, 3, 164-173.

[15] P. F. F. Almeida, A. Pokorny, and A. Hinderliter, Thermodynamics of membrane domains, Biochim. Biophys. Acta 1720 (2005) 1–13.

[16] H. J. Morowitz, Energy Flow in Biology, Ox Bow Press, (1968).
[17] V. J. Hilser, E. B. Thompson, Intrinsic disorder as a mechanism to optimize allosteric coupling in proteins, Proc. Natl. Acad. Sci. U.S.A. 104 (2007) 8311–8315.
[18] M. E. Fealey, J. W. Gauer, S. C. Kempka, K. Miller, K. Nayak, R. B. Sutton, and A. Hinderliter, Negative Coupling as a Mechanism for Signal Propagation between C2 Domains of Synaptotagmin I, PLoS One 7:e46748 (2012) 1-11.
[19] K. Fuson, A. Rice, R. Mahling, A. Snow, K. Nayak, P. Shanbhogue, A. G. Meyer, G. M. I. Redpath, A. Hinderliter, S. T. Cooper, and R. B. Sutton, Alternate Splicing of Dysferlin C2A Confers Ca(2+)-Dependent and Ca(2+)-Independent Binding for Membrane Repair, Structure 104 (2013) 104-115.
[20] J. W. Gauer, R. Sisk, J. R. Murphy, H. Jacobson, R. B. Sutton, G. D. Gillispie, and A. Hinderliter, Mechanism for Calcium Ion Sensing by the C2A Domain of Synaptotagmin I, Biophys. J. 103 (2012) 238–246.
[21] I. Letunic, T. Doerks, and P. Bork, SMART 7: recent updates to the protein domain annotation resource, Nucleic Acids Res. 40 (2011) D302–D305.
[22] A. Torrecillas, J. Laynez, M. Menéndez, S. Corbalán-García, J. C. Gómez-Fernández, Calorimetric Study of the Interaction of the C2 Domains of Classical Protein Kinase C Isoenzymes with Ca^{2+} and Phospholipids, Biochemistry 43 (2004) 11727-11739.
[23] J. W. Chen, P. Romero, V. N. Uversky, and A. K. Dunker, Conservation of Intrinsic Disorder in Protein Domains and Families: II. Functions of Conserved Disorder, J. Proteome Res. 5 (2006) 888–898.
[24] R. B. Gennis, Biomembranes: Molecular Structure and Function, 1st ed. New York, NY: Springer-Verlag, (1988).
[25] A. Hinderliter, P. F. F. Almeida, C. E. Creutz, and R. L. Biltonen, Domain Formation in a Fluid Mixed Lipid Bilayer Modulated through Binding of the C2 Protein Motif, Biochemistry 40 (2001) 4181–4191.
[26] A. Hinderliter, R. L. Biltonen, and P. F. Almeida, Lipid modulation of protein-induced membrane domains as a mechanism for controlling signal transduction, Biochemistry 43 (2004) 7102–7110.
[27] J. W. Gauer, K. J. Knutson, S. R. Jaworski, A. M. Rice, A. M. Rannikko, B. R. Lentz, and A. Hinderliter, Membrane Modulates Affinity for Calcium Ion to Create an Apparent Cooperative Binding Response by Annexin a5, Biophys. J. 104 (2013) 2437–2447.
[28] W. Cho, R. V. Stahelin, Membrane binding and subcellular targeting of C2 domains, Biochim. Biophys. Acta 1761 (2006) 838-849.
[29] J. Rizo, T. C. Südhof, C2-domains, Structure and Function of a Universal Ca2+-binding Domain, J. Biol. Chem. 274 (1998) 15879-15882.

[30] J. Xu, T. Bacaj, A. Zhou, D. R. Tomchick, T. C. Südhof, J. Rizo, Structure and Ca2+-Binding properties of the Tandem C2 domains of E-Syt2, Structure 22 (2014) 269-280.

[31] A. Bakan and I. Bahar, The intrinsic dynamics of enzymes plays a dominant role in determining the structural changes induced upon inhibitor binding, Proc. Natl. Acad. Sci. U.S.A. 106 (2009) 14349–14354.

[32] Y. Liu and I. Bahar, Sequence evolution correlated with structural dynamics, Mol. Biol. Evol. 29 (2012) 2253–2263.

[33] S. Takamori, M. Holt, K. Stenius, E. A. Lemke, M. Grønborg, D. Riedel, H. Urlaub, S. Schenck, B. Brügger, P. Ringler, S. A. Müller, B. Rammner, F. Gräter, J. S. Hub, B. L. De Groot, G. Mieskes, Y. Moriyama, J. Klingauf, H. Grubmüller, J. Heuser, F. Wieland, and R. Jahn, Molecular Anatomy of a Trafficking Organelle, Cell 127 (2006) 831–846.

[34] T. Brumm, The effect of increasing membrane curvature on the phase transition and mixing behavior of a dimyristol-sn-glycero-3-phosphatidylcholine/distearoyl-sn-glycero-3-phosphatidylcholine lipid mixture as studied by Fourier transform infrared spectroscopy and differential scanning calorimetry, Biophys. J. 70 (1996) 1373–1379.

[35] M. Ø. Jensen and O. G. Mouritsen, Lipids do influence protein function—the hydrophobic matching hypothesis revisited, Biochim. Biophys. Acta 1666 (2004) 205–226.

[36] A. A. Frazier, C. R. Roller, J. J. Havelka, A. Hinderliter, and D. S. Cafiso, Membrane-bound orientation and position of the synaptotagmin I C2A domain by site-directed spin labeling, Biochemistry 42 (2003) 96–105.

[37] E. Rufener, A. A. Frazier, C. M. Wieser, A. Hinderliter, and D. S. Cafiso, Membrane-Bound Orientation and Position of the Synaptotagmin C2B Domain Determined by Site-Directed Spin Labeling, Biochemistry 44 (2005) 18–28.

[38] J. Guillén, C. Ferrer-Orta, M. Buxaderas, D. Pérez-Sánchez, M. Guerrero-Valero, G. Luengo-Gil, J. Pous, P. Guerra, J. C. Gómez-Fernández, N. Verdaguer, S. Corbalán-García, Structural insights into the Ca2+ and PI(4,5)P2 binding modes of the C2 domains of rabphilin 3A and synaptotagmin 1, Proc. Natl. Acad. Sci. U.S.A. 110 (2013) 20503–20508.

[39] M. E. Fealey and A. Hinderliter, Allostery and instability in the functional plasticity of synaptotagmin I, Commun. Integr. Biol. 6:e22830 (2013) 1-4.

[40] Auluck, P. K., Caraveo, G., Lindquist, S. (2010) α-Synuclein: membrane interactions and toxicity in Parkinson's Disease. Cell Dev. Biol. 26, 211-233.

[41] Braun, A.R. and **Sachs, J.N.** α-Synuclein Stabilizes Small Unilamellar Vesicles By Reducing Both Membrane Surface Tension And Rigidity. *Biophys. J. Letters* 108, 1848-51. (2015)

[42] Rice, A. M., Mahling, R., Fealey, M. E., Rannikko, A., Dunleavy, K., Hendrickson, T., Lohese, K. J., Kruggel, S., Heiling, H., Harren, D., Sutton, R. B., Pastor, J., and Hinderliter, A. (2014) Randomly organized lipids and marginally stable proteins: A coupling of weak interactions to optimize membrane signaling, BBA Biomembranes, 1838: 2331-2340.

[43] Almeida, P. F., Best, A., Hinderliter, A. (2011) Monte carlo simulations of protein-induced lipid demixing in a membrane with interactions derived from experiment, Biophys J 101: 1930-1937.

[44] Braun, A. R., Sevcsik, E., Chin, P., Rhoades, E., Tristram-Nagle, S., and Sachs, J. N. (2012) alpha-Synuclein Induces Both Positive Mean Curvature and Negative Gaussian Curvature in Membranes, J Am Chem Soc 134: 2613-2620.